



MASTERS IN NANOTECHNOLOGIES FOR ICTS

MASTER THESIS

Bismuth-nanocomposites modified Screen Printed Carbon Electrodes for Non-Enzymatic Electrochemical Sensors

Mallikarjun Madagalam

Supervisors

Prof. Carrara Sandro (EPFL)
Prof. Alberto Tagliaferro (PoliTo)
Dr. Mattia Bartoli (PoliTo)

Bio/CMOS interfaces Group, Integrated Circuits Lab,
EPFL, Neuchâtel, Switzerland.

Carbon Group, DISAT, Politecnico di Torino, Italy.

July 10, 2020

Mallikarjun Madagalam

*Bismuth-nanocomposites modified Screen Printed Carbon Electrodes
for Non-Enzymatic Electrochemical Sensors* © February 2020

In the end, it's not the years in your life that count,
it's the life in your years.

— Abraham Lincoln

Dedicated to my family and friends.

*Everybody is a genius.
But if you judge a fish by
it's ability to climb a tree,
it will live it's whole life
believing that it is stupid.*

— Albert Einstein

Acknowledgements

I thank Prof. Carrara Sandro for giving me this excellent opportunity to work in Bio/CMOS interfaces group at EPFL under his supervision and helping me throughout this work with his valuable suggestions. I always felt like speaking with a friend whenever we had meetings and love to discuss anything with him, such a wonderful person I have ever met.

I would also like to thank my supervisor, Prof. Alberto Tagliaferro, at Politecnico Di Torino, who accepted me to work under his supervision in the Carbon group at Politecnico and his suggestions are always invaluable. I was also happy to work with Dr. Mattia Bartoli, who helped me throughout this project, starting from material synthesis at Polito. I am always grateful for his advice given to me whenever I asked him for help. I also thank Dr. Mahshid Padash for helping me in the chemical lab at the beginning of my project at EPFL.

I would like to express my gratitude to Ms. Bourquin Lysiane's administrative assistant of the Bio/CMOS group and Ms. Piffaretti Sandrine management assistant of IMT for helping me with all the administrative work regarding the mobility and bureaucracy.

Last but not least, I would like to thank my parents and friends who are always helping me throughout this masters program and everyone who was part of this beautiful journey.

Abstract

The main aim is to develop new non-enzymatic electrochemical sensors and study their performance in terms of the kinetic rate constant, sensitivity, and limit of detection. New sensors were developed by exploiting the functionalization of bismuth-composites on the surface of commercially available Screen Printed Carbon Electrodes. 12 different Bismuth composites based on HO-BiONO₃, with organic surfactants such as polyethylene glycol (PEG) and polyvinyl butyral (PVB) coatings to HO-BiONO₃, Bi₅O₇NO₃, and also Bismuth (Bi³⁺) coated Biochar (pyrolysis at 1000^oC) based materials were synthesized in carbon group at Politecnico Di Torino. Scanning electron microscopic experiments showed that different materials have different sizes and shapes. HO-BiONO₃ particles have been distributed with rod-shaped structure and Bi₅O₇NO₃ showed a sphere-like structure by forming aggregates. Commercially available Screen Printed Carbon Electrodes with carbon working electrode (area 0.12 cm²) and silver reference electrode were brought from DropSens. Homogeneous suspensions of all Bismuth-composites were prepared by using different solvents depending on their solubility. 5 μ L drops of each suspension were dispensed on the surface of different working electrodes and left them for drying (Drop casting technique). SEM images of the modified working electrodes showed that the synthesized particles on the surface got broken into smaller sizes with rectanguloid and cubic shapes with uniform distribution of particles. PEG-coated HO-BiONO₃ modified electrode's surface showed that most of the particles got stabilized by the PEG coating and remaining particles lost the coating since it is easy to remove PEG coating in aqueous solutions. Modified electrodes were used for electrochemical measurements of 1mM paracetamol in 0.1M PBS pH 7 by performing Cyclic Voltammetry with the help of AutoLab in Potentiostatic mode with the potential ranging from -0.4 V to 0.8 V vs Ag/AgCl at a scan rate of 100 mV/s. Observed that there is a significant improvement in oxidation peak currents compared to the bare or unmodified electrodes. Cyclic Voltammograms with the scan rates ranging from 50 mV/s to 300 mV/s in steps of 50 mV/s were also measured and demonstrated that the electrochemical system is a freely diffusing quasi-reversible system. Oxidation peak currents are linearly varying with the square root of scan rate and also oxidation and reduction peak positions varying linearly with the natural logarithm of scan rate. Slopes of these plots were used to find the electron transfer coefficient (α) and rate constant (k) with the help of the Laviron model. The diffusion coefficient (D) of paracetamol was also calculated at 100 mV/s using the Randles-Sevcik equation. Also, a cleaning procedure was followed by dipping modified SPCEs in 0.2M H₂SO₄ and performing a step of cyclic voltammetry in the potential range of -1.2V to 1.5V at 100 mV/s and observed higher oxidation peaks when measured 1mM paracetamol in 0.1M PBS pH 7 compared to the initial measurements but observed this in immediate measurements just after performing cyclic voltammetry in H₂SO₄.

Calibration curves were obtained by taking the oxidation peak currents with respect to the concentration (0.5mM to 3mM) and found the sensitivity of modified electrodes by taking the slope of the calibration curves. Higher sensitivity was observed for all modified electrodes compared to the unmodified electrode. Quantitatively, unmodified electrode has a sensitivity of $20.02 \pm 0.23 \mu A/mM$ with a limit of detection of 2.316 ± 0.026 mM ($R^2 = 0.994$, n=3) and a relative standard deviation

of 1.15%. Obtained maximum sensitivity for PEG-coated HO-BiONO₃ modified electrode was registered as more than double compared to unmodified electrode at the value of $43.50 \pm 0.54 \mu A/mM$ and limit of detection of 2.235 ± 0.028 mM ($R^2 = 0.998$, n=3) with relative standard deviation of 1.24%. Very low limit of detection was observed for PEG and PVB coated HO-BiONO₃ modified electrode at the value of 1.48763 ± 0.00037 mM. Further study on the interaction between Bismuth-composites and paracetamol by EDS measurements and electrochemical analysis by calculating the specific surface area of synthesized particles has been planned for the future.

Contents

List of Figures	ix
List of Tables	xii
Acronyms	xiv
1 Introduction	1
1.1 Electrochemistry of Biosensors	3
1.1.1 Kinetics of electron transfer	4
1.1.2 Mass transport	5
1.1.3 Cyclic Voltammetry	6
1.1.4 Laviron Equations	8
1.2 Electrochemical sensing of paracetamol	9
1.3 Bismuth based materials in biological applications	11
1.4 Project Aim	12
2 Materials and Methods	14
2.1 Materials Synthesis	14
2.1.1 Chemicals	14
2.1.2 Synthesis of HO-BiONO ₃	14
2.1.3 Synthesis of Bi ₅ O ₇ NO ₃	15
2.1.4 Synthesis of Bi ³⁺ /Biochar composites	15
2.2 Functionalization of Electrodes	16
2.2.1 Preparation of material suspensions	16
2.2.2 Electrodes modification	16
2.3 Preparation of Electrolytic Solution	16
3 Results and Discussions	18
3.1 Characterization of Materials	18
3.2 Surface characterization of SPEs	19
3.3 Electrochemical Measurements	21
3.3.1 HO-BiONO ₃ and Bi ₅ O ₇ NO ₃ modified electrodes	21
3.3.2 Cyclic Voltammetry in H ₂ SO ₄	29

3.3.3 Bi ³⁺ /Biochar modified electrodes	31
4 Conclusions	38
Bibliography	41

List of Figures

1.1	(a) Example of the three-electrode screen-printed sensor produced by BVT (Brno, Czech Rep.) . The sensor body is made from ceramics. (a) Working electrode (gold) is surrounded by (b) an Ag/AgCl reference electrode and (c) gold auxiliary electrode. Where d represents the silver contacts for output. The bottom scale is in millimeters[2]. (b) Another example of the three-electrode screen-printed sensor produced by Metrohm DropSens, Spain .The body is made from ceramic substrate (L33 x W10 x H0.5 mm) with carbon working electrode (area 0.12 cm ²), silver reference electrode, and carbon counter electrode. Different output connections are also shown.	2
1.2	Three-electrode electrochemical cell with nano/bio structures. W : Working Electrode, R : Reference Electrode, C : Counter Electrode [11].	3
1.3	(A) Homogeneous and (B) heterogeneous reduction of M1 ⁺ to M1. The energy of the electrons in the electrode is controlled by a potentiostat; their energy can be increased until electron transfer becomes favorable [12].	4
1.4	Cyclic voltammogram of the reversible reduction of a 1 mM Fc ⁺ solution to Fc, at a scan rate of 100 mV/s [12].	6
1.5	An example showing cathodic (red solid line) and anodic (blue solid line) linearly fitted peak potentials with ln(ν).	9
1.6	Skeletal formula of paracetamol (N-(4-hydroxyphenyl)ethanamide, C ₈ H ₉ NO ₂) [19].	10
1.7	Comparison of the electrochemical behavior in detection of paracetamol with some of the previously reported electrodes [29].	10
3.1	SEM images of (a) HO-BiONO ₃ material with a magnification of 10K ×, (b) PEG-coated HO-BiONO ₃ material with a magnification of 50K ×, and (c) Bi ₅ O ₇ NO ₃ material with a magnification of 200K ×.	18
3.2	Scanning electron micrograph of (a) the working surface of HO-BiONO ₃ modified SPE with a magnification of 10k × and (b) The details of HO-BiONO ₃ particles in 50k ×.	19
3.3	Scanning electron micrograph of (a) the working surface of PEG-coated HO-BiONO ₃ modified SPE with a magnification of 10k ×, (b) details with a magnification of 50k ×, (c) working surface of PEG-coated HO-BiONO ₃ modified SPE cleaned in 0.2M H ₂ SO ₄ with a magnification of 10k ×, and (d) details with a magnification of 50k ×.	20
3.4	Scanning electron micrograph of (a) the working surface of Bi ₅ O ₇ NO ₃ modified SPE with a magnification of 10k × and (b) details with a magnification of 50k ×.	20

3.5	Scanning electron micrograph of (a) the working surface of HO-BiONO ₃ 5% wt coated Bi ³⁺ /Biochar modified SPE with a magnification of 10k ×, (b) details with a magnification of 50k ×, (c) working surface of Bi ₅ O ₇ NO ₃ 5% wt coated Bi ³⁺ /Biochar modified SPE with a magnification of 10k ×, and (d) details with a magnification of 50k ×.	21
3.6	Cyclic voltammograms of 1 mM paracetamol in 0.1M PBS pH 7 at a scan rate of 100 mV/s with a) unmodified (bare) and b) HO-BiONO ₃ modified electrodes with different amounts of deposition (shown in legend).	22
3.7	Cyclic voltammograms of 1 mM paracetamol in 0.1M PBS pH 7 at a scan rate of 100 mV/s with HO-BiONO ₃ modified electrode and unmodified (bare) electrode. b) Possible oxidation mechanism of paracetamol [30].	22
3.8	Cyclic voltammograms of 1 mM paracetamol in 0.1M PBS pH 7 at a scan rate of 100 mV/s with (a) Bi ₅ O ₇ NO ₃ , HO-BiONO ₃ without surfactants modified and unmodified (bare) electrodes and (b) HO-BiONO ₃ with and without surfactants modified and bare electrodes.	23
3.9	Bare electrode : (a) Cyclic voltammograms of 1 mM paracetamol in 0.1M PBS pH 7 with different scan rates (50, 100, 150, 200, 250, and 300 mV/s), inset: redox peak currents with square root of scan rate, (b) redox peak positions with ln(scan rate) inset: peak-to-peak separation (ΔE_p) with ln(scan rate).	24
3.10	HO-BiONO ₃ modified electrode : (a) Cyclic voltammograms of 1 mM paracetamol in 0.1M PBS pH 7 with different scan rates (50, 100, 150, 200, 250, and 300 mV/s), inset: redox peak currents with square root of scan rate, (b) redox peak positions with ln(scan rate) inset: peak-to-peak separation (ΔE_p) with ln(scan rate). PEG-coated HO-BiONO ₃ modified electrode : (c) Cyclic voltammograms of 1 mM paracetamol in 0.1M PBS pH 7 with different scan rates (50, 100, 150, 200, 250, and 300 mV/s), inset: redox peak currents with square root of scan rate, (d) redox peak positions with ln(scan rate) inset: peak-to-peak separation (ΔE_p) with ln(scan rate).	25
3.11	95% confidence interval bound values (upper and lower bounds) for the peak potentials with ln(ν) for (a) HO-BiONO ₃ (b) PEG-coated HO-BiONO ₃ modified electrodes where purple, green, and cyan colored solid lines represent the fitted lines for cathodic lower bound, experimental, and upper bound potentials respectively and blue, red, and yellow colored solid lines represent the fitted lines for anodic lower bound, experimental, and upper bound potentials respectively.	26
3.12	Cyclic voltammograms of 0.5 mM to 3 mM paracetamol in 0.1M PBS pH 7 with (a) HO-BiONO ₃ and (b) PEG-coated HO-BiONO ₃ modified electrodes.	28
3.13	Calibration curves for different electrodes indicated in legends of (a) and (b).	29
3.14	Cyclic voltammograms of 1mM paracetamol in 0.1M PBS pH 7 at a scan rate of 100 mV/s with PEG-coated HO-BiONO ₃ modified electrode before and after each step of CV in 0.2M H ₂ SO ₄ (Corresponding voltammogram after each step is indicated in legend).	30
3.15	Cyclic voltammograms of 1 mM paracetamol in 0.1M PBS pH 7 at a scan rate of 100 mV/s with (a) unmodified, (b) HO-BiONO ₃ 5% Wt Bi ³⁺ /Biochar, (c) HO-BiONO ₃ 10% Wt Bi ³⁺ /Biochar, (d) HO-BiONO ₃ 15% Wt Bi ³⁺ /Biochar, (e) Bi ₅ O ₇ NO ₃ 5% Wt Bi ³⁺ /Biochar, (f) Bi ₅ O ₇ NO ₃ 10% Wt Bi ³⁺ /Biochar, and (g) Bi ₅ O ₇ NO ₃ 15% Wt Bi ³⁺ /Biochar modified electrodes.	31

3.16	HO-BiONO ₃ 5% Wt Bi ³⁺ /Biochar modified electrode: (a) Cyclic voltammograms of 1 mM paracetamol in 0.1M PBS pH 7 with different scan rates (50, 100, 150, 200, 250, and 300 mV/s), inset: redox peak currents with square root of scan rate, (b) redox peak positions with ln(scan rate) inset: ΔE_p with ln(scan rate). Bi ₅ O ₇ NO ₃ 5% Wt Bi ³⁺ /Biochar modified electrode : (c) Cyclic voltammograms of 1 mM paracetamol in 0.1M PBS pH 7 with same scan rates (50, 100, 150, 200, 250, and 300 mV/s), inset: redox peak currents with square root of scan rate, (d) redox peak positions with ln(scan rate) inset: ΔE_p with ln(scan rate).	32
3.17	Cyclic voltammograms of 0.5mM to 3mM (n=3) paracetamol in 0.1M PBS pH 7 at a scan rate of 100 mV/s with (a) HO-BiONO ₃ 5% Wt Bi ³⁺ /Biochar, (b) Bi ₅ O ₇ NO ₃ 15% Wt Bi ³⁺ /Biochar modified electrodes, and (c) Calibration curves for Bi ³⁺ /Biochar modified SPEs.	35
3.18	Cyclic voltammograms of 1 mM paracetamol in 0.1M PBS pH 7 at a scan rate of 100 mV/s after measurements with Bi ³⁺ /Biochar modified electrodes (shown in legend).	36

List of Tables

2.1	Amount of materials used for synthesis of HO-BiONO ₃	15
2.2	Exact amount of HO-BiONO ₃ and Bi ₅ O ₇ NO ₃ used to have 5%, 10%, and 15% wt of Bismuth (III) coated on 1g of Biochar.	15
2.3	Different solvents used for the preparation of homogeneous solutions.	16
3.1	Oxidation peak potentials and corresponding peak currents for different bare and modified electrodes.	23
3.2	Linear regression current equations with square root of scan rate and regression coefficients (R ²).	24
3.3	Linear regression peak potential equations with ln(ν) and regression coefficient (R).	25
3.4	Half potential (E _{1/2}) at a scan rate of 100 mV/s, electron transfer coefficient (α) and electron transfer number (n).	26
3.5	Linear regression peak-peak separation (ΔE_p) equations with ln(ν) and regression coefficient (R). ΔE_p values at a scan rate of 100 mV/s with standard deviations.	27
3.6	Rate constant (k) and diffusion coefficient (D) of paracetamol at a scan rate of 100 mV/s for bare and modified electrodes.	27
3.7	Linear regression equations of oxidation peak current with concentration (C) of analyte and their regression coefficients (R ²).	28
3.8	Sensitivity and Limit of detection (LOD) for bare and HO-BiONO ₃ and Bi ₅ O ₇ NO ₃ modified electrodes with their relative standard deviations (R.S.D).	29
3.9	Measured oxidation, reduction potentials and peak currents after CV in H ₂ SO ₄ for PEG-coated HO-BiONO ₃ modified electrode.	30
3.10	Oxidation peak potentials and corresponding peak currents for Bi ³⁺ /Biochar modified electrodes.	31
3.11	Linear regression peak current equations with square root of scan rate and regression coefficients (R ²) for Bi ³⁺ /Biochar modified electrodes.	33
3.12	Linear regression peak potential equations with square root of scan rate and regression coefficients (R) for Bi ³⁺ /Biochar modified electrodes.	33
3.13	Half potential E _{1/2} at a scan rate of 100 mV/s, electron transfer coefficient (α) and electron transfer number (n) for Bi ³⁺ /Biochar modified electrodes.	33
3.14	Linear regression equations of ΔE_p with ln(ν) and ΔE_p at a scan rate of 100 mV/s for Bi ³⁺ /Biochar modified electrodes.	34
3.15	Rate constant (k) and diffusion coefficient (D) at a scan rate of 100 mV/s for Bi ³⁺ /Biochar modified electrodes.	34

3.16 Linear regression equations of oxidation peak current with concentration for some Bi^{3+} /Biochar modified electrodes.	35
3.17 Sensitivities of some Bi^{3+} /Biochar modified electrodes.	35
3.18 Measured potentials and currents observed in after measurements.	36

Acronyms

SPCE Screen Printed Carbon Electrode

SPE Screen Printed Electrode

LSPR Localized Surface Plasmon Resonance

EPR Enhanced Permeation and Retention

PEG Poly Ethylene Glycol

PVB Poly Vinyl Butyral

HOMO Highest Occupied Molecular Orbital

LUMO Lowest Unoccupied Molecular Orbital

HLG HOMO LUMO Gap

POC Point-Of-Care

LOD Limit Of Detection

Chapter 1

Introduction

Nanomaterials and nanoparticles have gained more attention in technological advancements due to their tunable chemical, electrical, optical, and biological properties with improved performance when compared with the same materials with the larger size. There are different types of nanoparticles based on their size, shape, and surface properties. Nanoparticles can be synthesized based on a wide range of materials, and the most common materials are metals, metal oxides, ceramics, polymer materials, and compound semiconductors. They present several morphologies that are flakes, rods, flowers, and spheres. Nanoparticles are usually referred to as particles with a size of less than 100 nm in at least one dimension. Nanoparticles exhibit entirely new or improved properties based on their size, shape, and distribution [1]. Due to these unique properties of nanoparticles, a lot of research is going on cancer therapy, CT scanning, and targeted drug delivery. Apart from research in theranostic applications, nanoparticles are of very much interest in sensing applications, especially in electrochemical sensors and biosensors. Due to their size and shape, they can act as excellent catalytic agents and also provide better electron transfer properties. And quantum effects if the size of the particles falls in quantum regime¹. Nanoscale materials have been used extensively in electrochemistry over many years, to achieve high sensitivity and as low limit of detection (LOD) as possible by taking advantage of excellent catalytic and electron transfer properties of nanoparticles and also can provide very high active surface area depending on their size, shape, and distribution.

Electrochemical sensors have been the subject of interest and attracted more attention over decades due to their low cost, easy to realize and high selectivity, and their sensing ability to typical biomolecules such as Glucose, lactose, H₂O₂ and other molecules. Electrochemistry plays a pivotal role in the realization of these sensors and widely used in biomedical, pharmaceutical, and food industries. Many aspects have to be considered for mass production with high analytical performance. Electrochemical sensors can be of three different types depending on the sensing method. (i) Amperometric detection involves the electric current associated with electrons involved in redox reactions. (ii) Potentiometric detection measures the change in potential at electrodes due to ions or chemical reactions at an electrode. (iii) Conductometric detection measures the changes in resistance associated with the changes in the overall ionic medium between the electrodes [2]. Electrochemical biosensors were devices that respond to chemical reactions in a biological environment. Nowadays they are described as analytical devices composed of a biological recognition element directly interfaced with a signal transducer, which together relates the concentration of a targeted analyte or analytes to a measurable response [3, 4]. Biosensors have achieved and continue to gain attention because of their high sensitivity, specificity, ease for integration with other devices, and portability for utilization at on-site [5].

¹When the size of the particle is comparable with the electron De Broglie wavelength.

Nanotechnology and exploitation of new fabrication techniques offer simple, smaller, but robust sensing systems well suited for on-site analysis. Screen-printing technologies have provided just the kind of tool needed to take electrochemical biosensors towards point-of-care. Since the last two decades, screen-printing technology has exploited in biosensors. The production of highly reproducible, disposable, stable, and relatively low-cost SPEs, has had a profound impact on electrochemical biosensor development [6]. Screen-printing technology typically uses stencils, ink, and a squeeze blade. It is one of the leading technologies used in the push from lab to point-of-use. It is in large part due to their innate design of easily modifiable ink. Reference, working, and counter electrodes have given SPE an impeccable power of adaptability and excellent accuracy [7]. Also, SPEs have gained much interest because of the attractive features of carbon: chemically inert, low background currents, and larger potential window [7]. SPEs can be produced from many types of substrates with plastic films, ceramics, paper sheets, garments, stretch thin films, and epidermis. SPEs are typified by the fabrication of a three-electrode system on the same substrate [6]. An example of SPE is shown in figure 1.1a with the body made of ceramics with (a) gold working electrode surrounded by (b) Ag/AgCl (silver) reference electrode and (c) gold auxiliary electrode. Another example of the SPE sensor is shown in figure 1.1b with a body made of a ceramic substrate with dimensions of L33 x W10 x H0.5 mm. This SPE consists of a carbon working electrode (area 0.12 cm²), silver reference electrode, and carbon auxiliary/counter electrode.

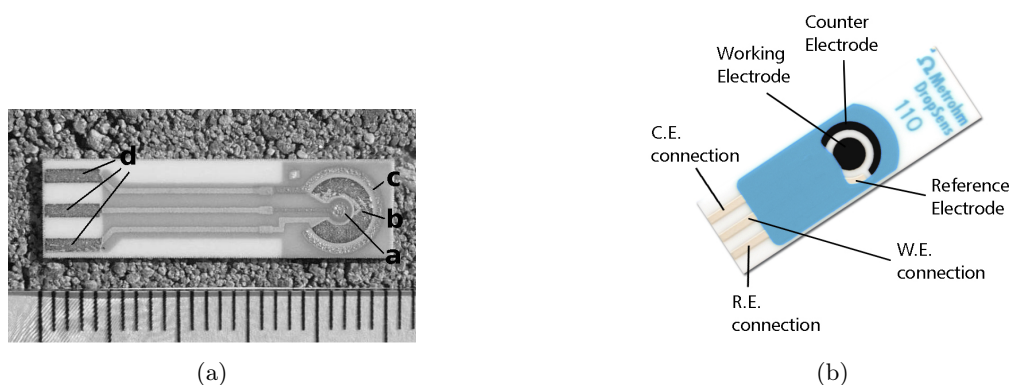


Figure 1.1: (a) **Example of the three-electrode screen-printed sensor produced by BVT (Brno, Czech Rep.)**. The sensor body is made from ceramics. (a) Working electrode (gold) is surrounded by (b) an Ag/AgCl reference electrode and (c) gold auxiliary electrode. Where d represents the silver contacts for output. The bottom scale is in millimeters[2]. (b) **Another example of the three-electrode screen-printed sensor produced by Metrohm DropSens, Spain**. The body is made from ceramic substrate (L33 x W10 x H0.5 mm) with carbon working electrode (area 0.12 cm²), silver reference electrode, and carbon counter electrode. Different output connections are also shown.

Another attractive feature of SPEs is that they can be surface-modified in the same way as conventional electrodes, thus enabling increased sensitivity when using superior electro-catalytic properties of nanoparticles. Moreover, they can be used with redox mediators to enhance the catalysis of targets that may otherwise not be easily analyzed due to their poor redox activity [8, 9, 10]. The whole work in this report is related to this attractive feature of SPEs shown in figure 1.1b and the study of electrochemical sensors performance when the surface of the SPEs is modified by using different materials.

1.1 Electrochemistry of Biosensors

Electrochemistry is defined as a branch of chemistry that examines the phenomena resulting from combined chemical and electrical effects. The typical electrochemical sensor is a three electrodes system with (i) a working electrode where the interesting phenomena happen, (ii) an auxiliary or a counter electrode which acts as a sink for current and helps in protecting the working electrode, and (iii) reference electrode which supports the voltage required by the current flow.

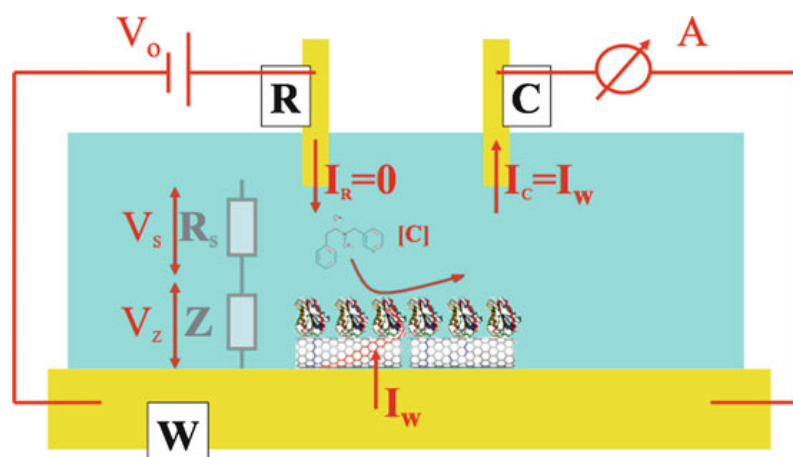


Figure 1.2: Three-electrode electrochemical cell with nano/bio structures. **W**: Working Electrode, **R**: Reference Electrode, **C**: Counter Electrode [11].

Figure 1.2 shows the typical three electrodes electrochemical biosensing system with nano/bio structures [11]. Electrochemistry typically involves the inflow of electrons due to chemical changes at the electrode and electrolyte interface. This chemical change is in the form of oxidation² or reduction³. These reactions are due to the electron transfer between the electrode and electrolyte molecules. When the electron transfer happens between two molecules due to energy difference in their energy levels is called homogeneous electron transfer and if this transfer is between an electrode and a molecule is termed as a heterogeneous transfer. But, how this transfer happens at the electrode and electrolyte interface? When we apply a voltage to the electrode with the help of a Potentiostat, the energy levels of electrons are modified then the electrons transfer happen between the electrode and molecular energy levels by tunneling. The energy difference between the electrode electron energy levels and the molecular energy levels act as a driving force responsible for this electron transfer. Homogeneous transfer of electrons between two molecules is called chemical reduction and heterogeneous transfer of electrons between electrode and molecule is called electrochemical reduction [12] due to the application of electrical voltage and these phenomena are shown in figure 1.3.

In a three-electrode electrochemical cell as shown in figure 1.2, the working and counter electrodes can be made of carbon, platinum, or gold and the reference electrode can be Ag/AgCl or saturated calomel electrode (SCE). These are typically used reference electrodes and all the electrochemical measurements have been done with respect to the reference electrodes. Electrochemical measurements involve the measurement of voltage, current, resistance, or some other property that is related to chemical species, and measurements are specific to the oxidation states of elements. We apply a voltage using a Potentiostat to the working electrode with respect to the reference electrode due to this voltage redox reactions happen at the interface of the working electrode and the chemical species in the form of electron transfer as shown in figure 1.3 and then

²Analyte (molecule or ion) loses one or more electrons

³Analyte (molecule or ion) gains one or more electrons

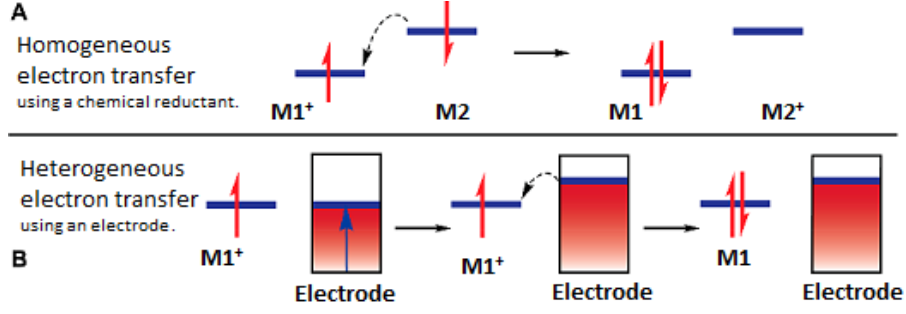


Figure 1.3: (A) Homogeneous and (B) heterogeneous reduction of $M1^+$ to $M1$. The energy of the electrons in the electrode is controlled by a potentiostat; their energy can be increased until electron transfer becomes favorable [12].

we measure the current between the working and the auxiliary/counter electrodes as shown in figure 1.2. It is possible to control the applied voltage between the working and the reference electrodes and change its values progressively until we observe a significant redox peak currents and corresponding potentials which are called redox potentials. These redox potentials can be changed depending on the type of reference electrode since the amount of energy required to make the redox reaction possible depends on the surface nature of the electrodes and the redox chemical species. Thus the standard potential and redox potentials depend on reference electrodes and redox species respectively.

1.1.1 Kinetics of electron transfer

Let us consider a general redox reaction at the electrode and electrolyte species interface



where k_f and k_b are the forward and backward kinetic rate constants with units of s^{-1} and are of the form

$$\begin{cases} k_b = k_b^0 e^{-\frac{\Delta G_b}{RT}} \\ k_f = k_f^0 e^{-\frac{\Delta G_f}{RT}} \end{cases}. \quad (1.2)$$

Where R is universal gas constant and T is absolute temperature. Rate constants with two different Gibbs free energies

$$\begin{cases} k_b = k_b^0 e^{-\frac{\Delta G_b^0 + \alpha n F (E - E^0)}{RT}} \\ k_f = k_f^0 e^{-\frac{\Delta G_f^0 - (1 - \alpha) n F (E - E^0)}{RT}} \end{cases}. \quad (1.3)$$

Equation 1.3 shows that forward and backward Gibbs free energies depend on the oxidation and reduction Gibbs free energies (ΔG_b^0 and ΔG_f^0), external energy (E) with respect to the standard potential (E^0), Faraday constant (F), electron transfer coefficient α that varies from 0 to 1 from reduction to oxidation respectively, and also on the number of electrons (n) participate in the reaction [11]. By definition, the perfect balance between a reduced and an oxidized species is obtained at a standard potential $E = E_0$ and $\alpha = 0.5$ then

$$k_b = k_f \Rightarrow k_b^0 e^{-\frac{\Delta G_b^0}{RT}} = k_f^0 e^{-\frac{\Delta G_f^0}{RT}} \equiv k^0. \quad (1.4)$$

From equations 1.3 and 1.4 we can write

$$\begin{cases} k_b = k_b^0 e^{-\frac{\alpha n F (E - E^0)}{RT}} \\ k_f = k_f^0 e^{\frac{(1-\alpha) n F (E - E^0)}{RT}} \end{cases} . \quad (1.5)$$

At the surface of the working electrode, the measured current is proportional to the concentration of oxidized and reduced species hence,

$$i = nFA[k_f C_O(0, t) - k_b C_R(0, t)]. \quad (1.6)$$

Where A is the area of working electrode, $C_O(0, t)$ and $C_R(0, t)$ are concentrations of oxidized and reduced species at the interface at time t. We can re-write equation 1.6 as

$$i = nFAk^0 \left[C_O(0, t) e^{-\frac{\alpha n F (E - E^0)}{RT}} - C_R(0, t) e^{\frac{(1-\alpha) n F (E - E^0)}{RT}} \right]. \quad (1.7)$$

Equation 1.7 is an important relationship between current and potential. It, or a variation derived from it, is used in the treatment of almost every problem requiring an account of heterogeneous kinetics [13]. These results and the inferences derived from them are known broadly as the Butler-Volmer formulation of electrode kinetics, in honor of the pioneers in this area [14]. At equilibrium, we have $i = 0$ then,

$$C_O(0, t) e^{-\frac{\alpha n F (E - E^0)}{RT}} = C_R(0, t) e^{\frac{(1-\alpha) n F (E - E^0)}{RT}} . \quad (1.8)$$

We get

$$\frac{C_O(0, t)}{C_R(0, t)} = e^{-\frac{n F (E - E^0)}{RT}} . \quad (1.9)$$

Equivalent to

$$\frac{n F (E - E^0)}{RT} = \ln \left[\frac{C_O(0, t)}{C_R(0, t)} \right]. \quad (1.10)$$

Finally it is possible to write an equation for external potential or energy E

$$E = E^0 + \frac{RT}{nF} \ln \left[\frac{C_O(0, t)}{C_R(0, t)} \right] \quad (1.11)$$

Equation 1.11 is called the Nernst equation from which we can obtain the reduction and oxidation peak potentials with respect to the change in concentration of redox species. The value of the electrode's potential depends not only on the concentration of species but also on the material of the electrode, the nature of the solvent, and temperature. Therefore the electrode potential is measured with respect to the reference electrode.

1.1.2 Mass transport

It has been noticed that the reaction rate can be changed by the electrode potential difference. However, the rate of transport to the surface can also affect or even dominate the overall reaction rate. For a fixed electrode area (A), the reaction rate can be controlled by two factors (i) the rate constant (k^0) and (ii) the surface concentration of the reactant ($C(0, t)$). If the rate constant is high, then any reactant close to the interface is immediately converted into a product such that the current will be controlled by the amount of fresh reactant reaching the interface from the bulk solution. The movement of the analytes at the electrochemical interface is important in predicting the current flow due to the concentration difference between the bulk and at the interface. The motion of ions from high to low concentration by diffusion is one of the forms of mass transport [11, 13]. The rate of diffusion can be understood mathematically with the help of Fick's laws of diffusion. By the first law of diffusion, the injected amount of redox species in the solution induces

a mass diffusion proportional to the variation in concentration in the sample. This mass flow is directional depending on the concentration gradient:

$$\vec{j}_m = -D\vec{\nabla}C(\vec{x}, t). \quad (1.12)$$

Where \vec{j}_m is the diffusion flux, D is the diffusion coefficient, negative sign defines the movement is from high to low concentration and $\vec{\nabla}C(\vec{x}, t)$ is the concentration gradient at distance x from the interface at time t . By Fick's second law it is instead possible to know the change in mass concentration with respect to time by the relation

$$\frac{\partial C(x, t)}{\partial t} = D \frac{\partial^2 C(x, t)}{\partial x^2}. \quad (1.13)$$

The rate of change of the concentration $C(x,t)$ as a function of time (t) is related to the change in the concentration gradient. So, higher is the change in concentration greater will be the rate of diffusion. In practice, diffusion is the most crucial transport process for many electrode reactions. Fick's second law is an important relationship since it permits the prediction of the variation of concentration of different species as a function of time within the electrochemical cell. To solve these expressions analytical or computational models are usually employed [11, 12].

1.1.3 Cyclic Voltammetry

Voltammetry is a technique used in electrochemistry to characterize electrochemical systems and acquire important information. Different voltammetric techniques are available such as linear sweep, differential pulse, square wave, and cyclic voltammetry. Cyclic voltammetry (CV) is a popular and most widely used technique to characterize an unknown electrochemical system. Which can provide reduction and oxidation peak potentials and corresponding peak currents due to the redox reactions between the electrode and the chemical species and also information about electron transfer based chemical reactions including catalysis [12].

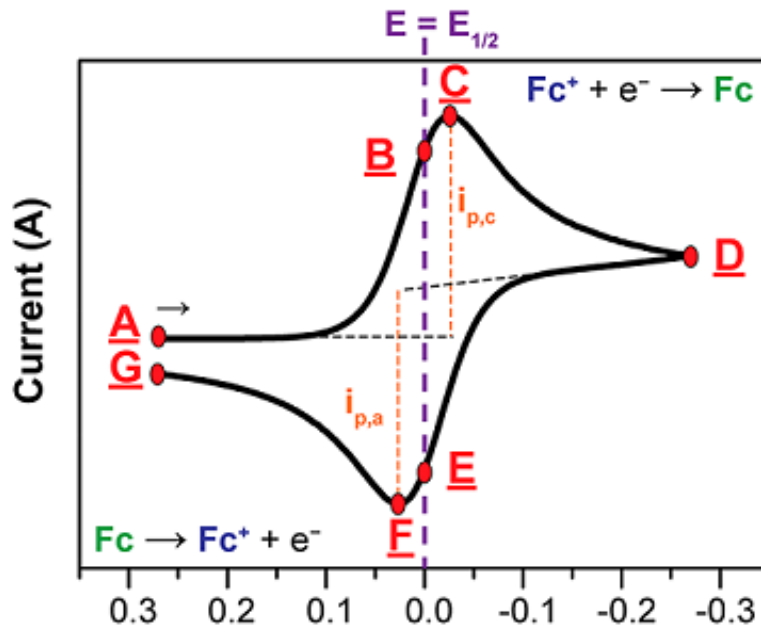


Figure 1.4: Cyclic voltammogram of the reversible reduction of a 1 mM Fc^+ solution to Fc , at a scan rate of 100 mV/s [12].

In cyclic voltammetry, we scan a voltage from negative to positive and also from positive to negative in a cyclic manner while continuously measuring the current between working and counter electrodes. We obtain a plot between applied potential and measured current and the plot looks like a duck-shaped one from which it is possible to extract the oxidation and reduction peak currents and corresponding potentials and these plots are generally called cyclic voltammograms. A typical shape of a cyclic voltammogram is shown in figure 1.4.

To obtain the data in figure 1.4, the voltage was scanned from 0.3 V to -0.3 V (A to D) and then back from -0.3 V to 0.3 V (D to G) as a function of time at a scan rate of 100 mV/s. As potential decreases, electrode reaction becomes more strongly reducing ($Fc^+ \rightarrow Fc$) and reduction current increases, when the potential increases, electrodes reaction becomes more strongly oxidizing ($Fc \rightarrow Fc^+$) and oxidation current increases. But, why the oxidation or reduction currents keep on increasing with voltage increase or decrease? why do we observe a peak current at point C and point F? This shape is due to two effects (i) the Nernst equation: reduction won't occur until the applied potential is sufficiently reducing from equation 1.10 and rearrange it

$$\ln \left[\frac{C_R(0,t)}{C_O(0,t)} \right] = \frac{nF}{RT} (E^0 - E). \quad (1.14)$$

Where E is the potential at the working electrode and $E^0 = E^{\frac{1}{2}}$ (in fig.1.4) is the standard potential of this redox couple and reduction occurs only when $E < E^{0.4}$. (ii) After the reduction current reaches a peak $i_{p,c}$ at C it starts to decrease due to the effect of analyte depletion by slow diffusion. The Nernst equation applies only for a certain range of nanometers away from the interface into the analyte species. Current depends on the rate at which the analyte can diffuse to the surface of the working electrode. Due to these two effects, the redox currents take that shape but why doesn't the current go-to zero? This current is called non-Faradaic current due to charge accumulation at electrode surface (non-Nernstian) so, we subtract this non-Faradaic current as background from the total current to obtain the exact oxidation and reduction peak currents. This can be done by baseline correction in subtracting the non-Faradaic current to extract only the Faradaic current due to the electron transfer at the interface (Nernstian) as shown in figure 1.4. Where $i_{p,c}$ and $i_{p,a}$ are cathodic (reduction) and anodic (oxidation) peak currents which are measured to the points C and F, respectively by drawing straight lines to the corresponding bases. For an ideal reversible electrochemical system, after the background correction, the ratio between oxidation peak current and reduction peak current is equal to 1 [12].

Importance of scan rate

The scan rate is how fast the potential is applied between the working and reference electrodes. Faster scan rates lower the size of the diffusion layer hence higher currents can be observed [13]. For an electrochemically reversible electron transfer processes involving freely diffusing redox species, the Randles-Sevcik equation describes how the peak current i_p (A) increases linearly with the square root of the scan rate ν (V/s),

$$i_p = 0.446nFAC \left(\frac{nF\nu D}{RT} \right)^{\frac{1}{2}}. \quad (1.15)$$

Where n is the number of electrons transferred in the redox reaction, A (cm^2) is the electrode geometric surface area, D (cm^2/s) is the diffusion coefficient of the oxidized analyte, and C (mol/cm^3) is the bulk concentration of the analyte. The Randles-Sevcik equation can give indications on whether an analyte is freely diffusing in solution or adsorbed on the surface of the electrode. For electrochemically reversible electron transfer processes involving freely diffusing redox species,

⁴ E^0 is the half difference between reduction and oxidation potentials when measured with standard reference electrode.

the Randles-Sevcik equation reveals that the plots of i_p versus $\nu^{1/2}$ should be linear. For an electrode-adsorbed species, the current response is described by:

$$i_p = \frac{n^2 F^2}{4RT} \nu A \Gamma^* \quad (1.16)$$

Where Γ^* is the surface coverage of the adsorbed species in mol/cm². The current response expected to be varied linearly with ν . For an analyte that is thought to be a freely diffusing species, deviations from linearity in plots of i_p vs. $\nu^{1/2}$ suggest either (a) electrochemical quasi-reversibility or (b) that electron transfer may be occurring via surface-adsorbed species. It can be understood by taking the peak-to-peak separation into account if the peak positions are shifting with the scan rate then the system is quasi-reversible whereas in surface-adsorbed cases no peak positions shifting will be observed. Also, the Randles-Sevcik equation may be used to calculate diffusion coefficients [12].

1.1.4 Laviron Equations

In 1979, E.Laviron [15] proposed a general expression to determine the kinetic rate constant (k) and electron transfer coefficient (α) in the case of linear potential sweep voltammogram techniques for diffusionless electrochemical systems which means without taking any diffusion effects into account. After some general considerations and calculations (see. [15]) ended up with the cathodic peak potential

$$E_{p,c} = E^0 - \left(\frac{RT}{\alpha n F} \right) \ln \left[\frac{\alpha}{|m|} \right], \quad (1.17)$$

and anodic peak potential

$$E_{p,a} = E^0 + \left(\frac{RT}{(1-\alpha)nF} \right) \ln \left[\frac{(1-\alpha)}{|m|} \right]. \quad (1.18)$$

Where α is the electron transfer coefficient and

$$m = \left(\frac{RT}{F} \right) \left(\frac{k}{n\nu} \right) \quad (1.19)$$

where $k = k_s$ as homogeneous rate constant or $k = Ak_{s,h}/V$ with $k_{s,h}$ as heterogeneous rate constant (s^{-1}) and V as volume. He characterized the nature of the electrochemical system based on m as $m \rightarrow \infty (\nu \rightarrow 0)$, both cathodic and anodic peaks tend to be "reversible" and symmetrical with the potential axis. When $m \rightarrow 0 (\nu \rightarrow \infty)$ the peaks tend to be "totally irreversible". Experimentally two conditions have been found to determine α and k_s by taking the difference between anodic and cathodic peaks positions ΔE_p into account. if $n\Delta E_p > 200mV$ can be found experimentally, then α , k can be calculated by using the equations 1.17 and 1.18. If we plot the peak positions versus $\ln(\nu)$ which gives two straight lines with slopes equal to $-RT/\alpha nF$ for cathodic peak, and $RT/(1-\alpha)nF$ for anodic peak. α can be found from the slopes and k can be calculated by using the equation

$$\log k = \alpha \log(1-\alpha) + (1-\alpha) \log \alpha - \log(RT/nF\nu) - \alpha(1-\alpha)nF\Delta E_p/2.3RT. \quad (1.20)$$

This is valid only for $n\Delta E_p > 200mV$. For example, figure 1.5 shows the cathodic (red solid line) and anodic (blue solid line) linearly fitted peak potentials with $\ln(\nu)$.

The slope of the cathodic fit is $Sc = -31.83$ and the anodic fit is $Sa = 15.56$. By equating these slopes to the equations mentioned above we get

$$31.83(\alpha nF) = 15.56(1-\alpha)nF.$$

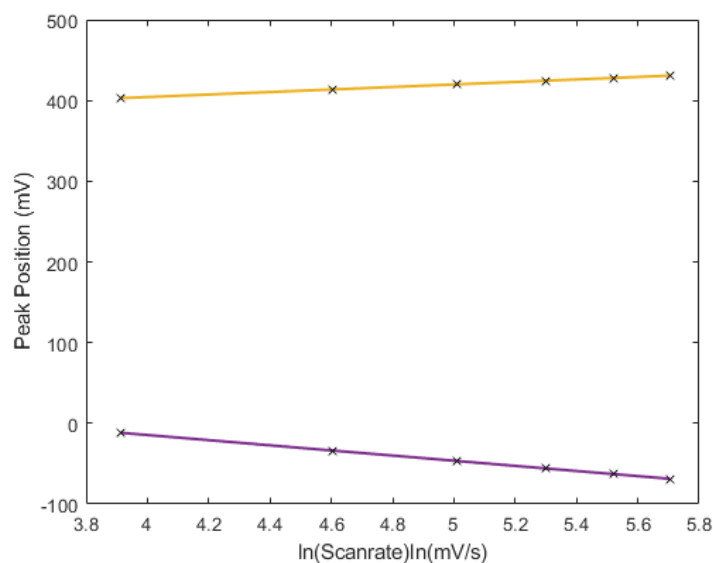


Figure 1.5: An example showing cathodic (red solid line) and anodic (blue solid line) linearly fitted peak potentials with $\ln(\nu)$.

By cancelling the terms on both sides and bringing α terms into one side we have

$$\alpha = 15.56/47.39 = 0.33.$$

We know the peak-to-peak separation $\Delta E_p=447.39$ mV, $n=2$, $\nu=100$ mV/s, $R=8.314$ J/mol.K, $F=96485.3329$ s.A/mol, and $T=300$ K. We have $n\Delta E_p > 200mV$ therefore we can substitute these values respectively into the equation 1.20 and solve for the rate constant (k), we get $k=1.5$ ms^{-1} .

If $n\Delta E_p < 200mV$ find experimentally, then α can in principle be determined from the graph $y = |(E_{p,c} - E^0)/(E_{p,a} - E^0)|$, provided that E^0 can be determined by extrapolation of the curves $nE = f(\nu)$, in this case α won't be a precise value and only an approximate value can be determined using different curves present in [15] and then m and k will be easily calculated. One can refer [15] for example, in this case, to calculate the values of α and rate constant (k). Note that Laviron equations are applied only by assuming that there is no diffusion of species in the electrochemical system, meaning that in the absence of double-layer effects while the calculation of rate constant will be greatly influenced by the presence of double-layer effects [16].

1.2 Electrochemical sensing of paracetamol

Within the frame of present master thesis work, we are going to use paracetamol as a kind of "probe molecule" (or as a molecular model) to establish the performance of our surfaces once used in electrochemical sensing. Paracetamol is a commonly used drug for relief from fever, headache, toothache, migraine, cold and chronic pain it is also widely used as an antipyretic and analgesic drug [17, 18], and the skeletal formula of paracetamol is shown in figure 1.6.

Paracetamol is also known as acetaminophen, N-acetyl-p-aminophenol which is a safe agent and very effective when we use within limits but sometimes overdose and chronic use can cause toxic metabolite accumulation which can damage liver and kidney [20]. Hence, an accurate, fast, simple, sensitive, and easily applicable method is needed to determine the levels of the paracetamol in

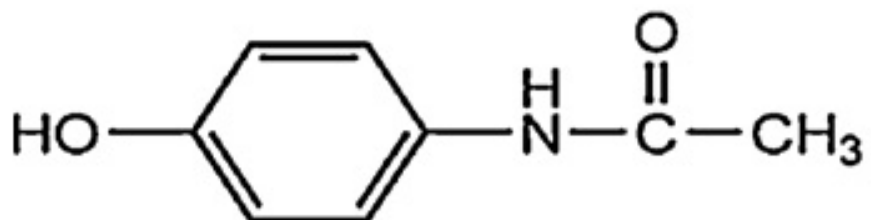


Figure 1.6: Skeletal formula of paracetamol (N-(4-hydroxyphenyl)ethanamide, $C_8H_9NO_2$) [19].

pharmaceutical applications and biological fluids (urine, blood, or plasma). Different analytical methods have been proposed such as spectrophotometry [21, 22], titrimetry [23], liquid chromatography [24], chemiluminescence [25], capillary electrophoretic methods [26], water analysis [27] and electroanalytical methods [28]. These methods involve tedious processes with time-consuming so, we need a simple and fast response system that is possible with electrochemical techniques that are extensively used accurate, fast, highly sensitive, cost-effective, and applicable at the point-of-care (POC). These techniques are well known in pharmaceutical, food industries, and biological fields due to their simplicity and on-site application. Since the paracetamol is electroactive, electrochemical sensing techniques are most suitable for the determination of levels of the paracetamol than the above-mentioned methods that are extensively used in pharmaceutical applications to determine paracetamol.

Electrode	pH	E_p vs. Ag/AgCl (V)	Linear range (μ M)	DL (μ M)
C-Ni/GCE	BR, pH 3	+0.733 (vs.SCE)	7.8–110	–
Cu-PTTCA/GCE	PBS, pH 7	+0.65	20–5,000	5
PGE	pH 6.5 ^a	+0.492 (vs.SCE)	1–8, 20–100	0.0142
CPE	PBS, pH 7.2	+0.96 (vs.SCE)	1–1,000	0.5
Nafion/ROP/GCE	M HClO ₄	+1.45	50–2500	1.2
C ₆₀ /GCE	PBS, pH 7.2	–	50–1,500	50
VCPTe	PBS, pH 7	–	0.120–5,800	88
MWNTs/GCE	–	–	0.4–150	0.12
SWNT-DCP/GCE	PBS, pH 6.5	+0.36 (vs.SCE)	0.1–20	0.04
PAN/MWCNTs/GCE	M ABS	+0.436 (vs.SCE)	1–100, 250–2,000	0.25
Nafion/GCE	Solution ^b	–	50–500	17
GCE	PBS, pH 7	–	2–1,580	19
MIP/PGE	PBS, pH 7	+0.450	5–500, 1,250–4,500	0.79
Pt electrode	M H ₂ SO ₄	+0.835 (vs.SCE)	4–100	1
Nanogold/ITOE	PBS, pH 7.2	+0.830	0.2–1,500	0.18
CILE	ABS, pH 4.6	+0.462 (vs.SCE)	1.0–2,000	0.3

Figure 1.7: Comparison of the electrochemical behavior in detection of paracetamol with some of the previously reported electrodes [29].

Nanomaterials immobilized electrodes have been widely used in electrochemical techniques to detect paracetamol, a lot of research has been already done based on different nanomaterials modified electrodes because of their unusual and unique electronic and catalytic properties. Many methods have shown very good sensitivity, stability, selectivity, and a very low level of detection due to the excellent properties of nanomaterials used for the functionalization of electrodes. Figure 1.7 shows the important results obtained by previous research on electrochemical sensing of paracetamol based on different materials immobilized on the surface of the working electrode.

Some of the previous materials used to develop sensors for the sensing of paracetamol include Bi₂O₃ nanoparticles [30], "Bismuth particles Nafion covered boron-doped diamond electrodes" [31], Carbon nanotubes [32], graphene based [18], Nafion/TiO₂-graphene [26], carbon ionic liquids [29] and also other materials shown in above figure 1.7.

1.3 Bismuth based materials in biological applications

Bismuth (Bi, $z = 83$) attracted further interest in recent years and especially in the fields of nanotheranostic drug delivery, nanomedicine, food safety, biochemistry and pharmaceutical applications. Different Bismuth based compounds have been synthesized and used as photocatalytic agents in CT imaging, nanotherapeutic drug delivery in cancer therapy *in vitro*, and *in vivo*, and hyperthermia treatment. Photocatalytic agents can help in converting light energy into thermal energy (heat) to kill cancer cells in hyperthermia treatment. Materials with near-infrared (NIR) absorption can act as excellent photothermal agents such as hydrophilic flower-like Bismuth sulfide (Bi_2S_3) superstructures covered with polyvinylpyrrolidone (PVP) exhibited a very high photothermal conversion efficiency of about 64.3% [33] and also bovine serum albumin (BSA) mediated Bi_2S_3 sub 10 nm particles as "Nanotheranostic Agents for Tumor Multimodal Imaging and Thermoradiotherapy". Due to the narrow direct bandgap (≈ 1.3 eV), Bismuth sulfide exhibits strong NIR absorbance that makes Bi_2S_3 NPs potentially useful, also, Bi_2S_3 NPs were exploited as CT contrast agent because of the large X-ray attenuation coefficient of Bismuth element owing to its high atomic number [34]. PEGylated Bi-nanocrystals for *in vivo* multimodal bio-imaging and as photothermal agents [35], Bismuth Selenide (Bi_2Se_3) topological insulator in X-ray computed tomography cancer imaging and therapy [36], and black phosphorous/ Bi_2O_3 nanosheet heterostructures as "effective and biocompatible radiosensitizers for synergistic cancer radiotherapy and showed good biocompatibility *in vitro* and *in vivo*" [37]. Bismuth is considered one of the most biocompatible elements with low toxicity and good tolerance at high doses amongst the transition metals [33, 38] and used in commercial applications as "Bismuth therapy" drugs for many diseases [33, 39].

Many other Bismuth based compounds possess good photocatalytic characteristics due to their narrow band gap (< 2.9 eV) such as Bi_6WO_6 , Bi_2MoO_6 , BiVO_4 [40], Bismuth Oxyhalides (BiOX , $X = \text{F}, \text{Cl}, \text{Br}, \text{I}$), $\text{Bi}_5\text{O}_7\text{I}$ and $\text{Bi}_5\text{O}_7\text{NO}_3$ ($E_g = 2.7 - 2.9$ eV) [41].

Bismuth based research in electroanalysis has started in 20th-century [42, 43, 44], which was considered as the "classical era" where they covered the research in metal/metal oxide electrodes for pH sensing and the most successful inventions were the Bi/ Bi_2O_3 electrodes. "A Decade with Bismuth-Based Electrodes in Electroanalysis [45]" has reported the achievements at the beginning of the 21st century so-called "modern era" starting from 2000. In which they have reported the advancements with Bismuth based electrodes as a replacement to mercury electrodes which have dominated the electrochemical stripping analysis for many decades. In the year 2000, Bismuth coated carbon electrodes were invented by Joseph Wang et al [46] as a replacement for mercury electrodes for anodic stripping voltammetry. The actual view behind this invention was to use Bismuth (III) as a new "green" standard in "green chemistry", because of its versatile, environmentally friendly, low toxicity, not responding to the presence of oxygen, mechanical stability in different forms and excellent ability to couple with inert electrode substrates such as carbon electrodes and electrochemical characteristics favorable in both faradic and non-faradic measurements [45]. Since then it has been an excellent scientific ride for Bismuth modified electrodes, sensors, and different detection techniques.

The potential of Bismuth film electrodes in organic electroanalysis has been determined by [47]. The glassy carbon electrodes that were dominating the electrochemical stripping analysis have been replaced by the Bismuth modified screen-printed electrodes [48] in 2001. Dual role for Bismuth (III) ions was revealed in 2002 [49] by giving indications for special applications through electrocatalytic effect in highly sensitive detection [50]. The first real-life biological application of Bismuth film electrodes [51] and many other achievements through those years lead to the formation of an imaginary association called "Bismuth club" in 2006. The very first mention of Bismuth electrodes with "nanoscale" in electroanalysis [52] was mentioned in 2007 by continuing the boom of Bismuth in electroanalysis. A lot of attention for preparation of Bi-nanoparticles by

using some special procedures, screen printed Bi-nanoparticle electrodes through electrochemical reduction of Bi_2O_3 [53]. Many other noticeable achievements in this decade from 2000-2010, Bismuth electrodes have widened their scope in electroanalysis and electrochemical biosensors as they are non-toxic and can be operated in the presence of oxygen.

Bismuth is widely used in electrochemical sensors for biomolecules sensing due to its efficient electron charge transfer [54] and acts as a good electrocatalyst. Bismuth containing nanocomposites have been extensively used in non-enzymatic electrochemical sensors for biomolecules sensing. Multi-walled carbon nanotube/poly(pyrocatechol violet)/Bi film [55], biochar/Bi nanostructures/carbon composite [56], and Bi-Ag bimetallic nanoparticles [57] have been developed and used in sensing of heavy metal ions[40]. Recently developed HO-BiONO₃ nanocomposites modified GCE in non-enzymatic electrochemical sensing of Glucose [40], Bi_2O_3 nanoparticles modified SPEs in sensing H_2O_2 [58], Bi_2O_3 nanoparticles modified GCE [30] in determining paracetamol and "Bismuth particles Nafion covered boron-doped diamond electrode for simultaneous and individual voltammetric assays of paracetamol and caffeine" [31].

1.4 Project Aim

The main aim of the present work was to synthesize different Bismuth-composites and use them in the development of new non-enzymatic electrochemical sensors based on Screen Printed Carbon Electrodes (SPCEs). SPEs have been surface modified and they have been used as electrochemical sensors in sensing paracetamol through cyclic voltammetric measurements. The performance of these newly developed electrochemical sensors has been studied in terms of rate constant (k), sensitivity, and limit of detection. Along this thesis, all these parameters have been calculated with experimental data and then compared among different newly developed sensors to find the best sensor which can be used in control processes.

In later chapters, synthesis of materials and methods used, characterization of synthesized materials and results of electrochemical measurements, followed by some important conclusions have been presented, respectively.

Chapter 2

Materials and Methods

Bismuth based composite materials used in this project were synthesized in Carbon Group at Politecnico Di Torino, with the help of Dr. Mattia Bartoli and following the literature [40, 59, 60]. Modification of electrodes and electrochemical measurements have been performed in Bio/CMOS interfaces group at EPFL, Switzerland.

2.1 Materials Synthesis

2.1.1 Chemicals

Bismuth nitrate pentahydrate ($\text{Bi}(\text{NO}_3)_3 \cdot 5\text{H}_2\text{O}$), Butyl alcohol ($\text{C}_4\text{H}_{10}\text{O}$), Biochar (already Pyrolysed at 1000°C), Acetone ($(\text{CH}_3)_2\text{CO}$), Polyethylene glycol (PEG), Polyvinyl butyral (PVB) were used for material synthesis at Politecnico di Torino. Dimethyl sulfoxide - DMSO ($(\text{CH}_3)_2\text{SO}$), Methanol (CH_3OH), H_2SO_4 , Phosphate buffer saline (PBS), DI water and paracetamol tablets made into powder were used for the preparation of material suspensions and electrolytic solution at EPFL.

2.1.2 Synthesis of HO-BiONO_3

HO-BiONO_3 was synthesized by a simple method adapted from literature [40, 59]. $\text{Bi}(\text{NO}_3)_3 \cdot 5\text{H}_2\text{O}$ was mixed with butanol ($\text{C}_4\text{H}_{10}\text{O}$) with a weight ratio of 1:12. The mixture was kept in an ultrasonic bath while constantly stirring for 1 hour to achieve a homogeneous suspension. After that, the suspension was kept inside a drying oven at 150°C for 5 hours to obtain HO-BiONO_3 material.

In another beaker, the same mixture of $\text{Bi}(\text{NO}_3)_3 \cdot 5\text{H}_2\text{O}$ and butanol with a weight ratio of 1:12 was prepared. Unlike the previous case, the mixture was kept under a tip sonicator for an 'ON' time of 15 minutes and a total period of 22-25 minutes to acquire a homogeneous suspension. Later the suspension was kept inside a drying oven at 150°C for 5 hours to achieve HO-BiONO_3 material while expecting a different particle size from the previous case.

Synthesis with Organic Coatings

Again the same mixture with 1:12 weight ratio was prepared but also polyethylene glycol (PEG) was added with a 1:1 weight ratio of PEG and $\text{Bi}(\text{NO}_3)_3 \cdot 5\text{H}_2\text{O}$. This mixture was kept under a tip sonicator for an 'ON' time of 15 minutes and for a total period of 22-25 minutes to prepare

a homogeneous suspension. This suspension was kept inside a drying oven for 5 hours to obtain PEG-coated HO-BiONO₃ powder.

A mixture with a weight ratio of 1:12 Bi(NO₃)₃.5H₂O and butanol, and a weight ratio of 1:1 Bi(NO₃)₃.5H₂O and Polyvinyl butyral (PVB) was prepared, and then tip sonication and drying as in the previous case. The final product was a yellow-colored hard solid substance which was ground to acquire PVB-coated HO-BiONO₃ powder-like substance.

Finally to have PEG and PVB-coated HO-BiONO₃ material, a mixture with Bi(NO₃)₃.5H₂O, butanol, PEG and PVB with same weight ratio as before and followed the same procedure of tip sonication and drying. Table 2.1 shows the amounts of all the materials used for the synthesis of HO-BiONO₃ composite materials.

Material synthesized	Bi(NO ₃) ₃ .5H ₂ O (g)	C ₄ H ₁₀ O (mL)	PEG (g)	PVB (g)
HO-BiONO ₃	10.506	125	-	-
HO-BiONO ₃ TS	10.511	126	-	-
PEG coated HO-BiONO ₃	10.506	126	10.503	-
PVB-coated HO-BiONO ₃	10.506	126	-	10.527
PEG, PVB-coated HO-BiONO ₃	10.506	126	10.504	10.524

Table 2.1: Amount of materials used for synthesis of HO-BiONO₃.

2.1.3 Synthesis of Bi₅O₇NO₃

Inspired by the research of Kodama[60], Bi₅O₇NO₃ was synthesized by solid-state thermal decomposition. In three small ceramic bowls, 10.1032 g, 10.2050 g, and 10.1295 g of Bi(NO₃)₃.5H₂O weighed and kept in an oven. The temperature inside the Oven was increased from room temperature to 400⁰C in steps of 10⁰C/min, then the samples were taken out and cooled down to room temperature to achieve Bi₅O₇NO₃ powder. In total, 30.438 g of Bi(NO₃)₃.5H₂O used to obtain 16.875 g of Bi₅O₇NO₃ hence a yield of around 50% of the total weight.

2.1.4 Synthesis of Bi³⁺/Biochar composites

Bi³⁺/Biochar composite materials also were synthesized to have 5%, 10%, and 15% weight of Bismuth (III) in 1 gram of Biochar that was obtained by pyrolysis at 1000⁰C. HO-BiONO₃ has 68.74% weight of Bismuth, and Bi₅O₇NO₃ has 85.72% weight of Bismuth in their composition. Table 2.2 shows the amount of HO-BiONO₃ and Bi₅O₇NO₃ used to have 5%, 10%, and 15% wt of Bismuth coated on 1g of Biochar.

Material synthesized	Biochar (g)	HO-BiONO ₃ (g)	Bi ₅ O ₇ NO ₃ (g)
HO-BiONO ₃ 5% Wt Bi ³⁺ /Biochar	1.0054	0.0781	-
HO-BiONO ₃ 10% Wt Bi ³⁺ /Biochar	1.0278	0.1631	-
HO-BiONO ₃ 15% Wt Bi ³⁺ /Biochar	1.0620	0.1762	-
Bi ₅ O ₇ NO ₃ 5% Wt Bi ³⁺ /Biochar	1.0230	-	0.0625
Bi ₅ O ₇ NO ₃ 10% Wt Bi ³⁺ /Biochar	1.0133	-	0.1302
Bi ₅ O ₇ NO ₃ 15% Wt Bi ³⁺ /Biochar	1.0120	-	0.2083

Table 2.2: Exact amount of HO-BiONO₃ and Bi₅O₇NO₃ used to have 5%, 10%, and 15% wt of Bismuth (III) coated on 1g of Biochar.

Previously synthesized HO-BiONO₃ and Bi₅O₇NO₃ were mixed with Biochar as per the table 2.2 in six different beakers and 20 mL of acetone was added to each beaker. All beakers were kept

in an ultrasonic cleaner while constantly rinsing for a half-hour to have homogeneous solutions. Then the solutions were kept in a drying oven at 60°C for 2-3 hours until the samples become completely dry. This is how Bi³⁺/Biochar composite materials were obtained.

2.2 Functionalization of Electrodes

2.2.1 Preparation of material suspensions

Inspired by Gen-qing Liu et al[40], homogeneous suspensions were prepared for all synthesized materials by using different solvents shown in table 2.3 depending on their solubility. Materials and solvents were added in a 3:1 ratio and kept in the ultrasonic bath until they became homogeneous solutions.

Material	Solvent used
HO-BiONO ₃ (12mg)	Distilled Water (4 mL)
Bi ₅ O ₇ NO ₃ (12mg)	Distilled Water (4 mL)
PEG coated HO-BiONO ₃ (3mg)	Distilled Water (1 mL)
PVB-coated HO-BiONO ₃ (12mg)	Methanol (4 mL)
PEG & PVB-coated HO-BiONO ₃ (12mg)	Methanol (4 mL)
Bi ³⁺ /Biochar composites (12mg)	Dimethyl Sulfoxide (DMSO) (4 mL)

Table 2.3: Different solvents used for the preparation of homogeneous solutions.

2.2.2 Electrodes modification

Screen-printed electrodes with carbon working electrode (area 0.12 cm²), carbon counter electrode, and silver reference electrode were used as electrochemical sensors. Electrodes were modified by spreading 5 μL drops of each suspension on the surface of the working electrode and drying at room temperature (drop-casting technique). But, in the case of Bi³⁺/Biochar composites, electrodes were kept on a hot plate at around 60°C then the suspension was spread on the working electrode in steps of 2 μL, 2 μL, and 1 μL because Dimethyl Sulfoxide (DMSO) has relatively high boiling and freezing points so that it evaporates very slowly in atmospheric conditions. 12 different screen printed electrodes were modified by using different Bismuth-based composites.

2.3 Preparation of Electrolytic Solution

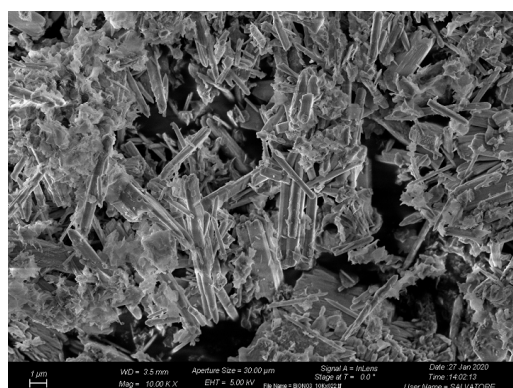
5mM paracetamol in Phosphate buffer saline (PBS) at pH 7 was prepared by adding 3.78g of paracetamol to 5mL of 0.1M PBS solution. Then the solution was diluted to 1mM paracetamol in 0.1M PBS at pH 7 by adding 0.2mL of 5mM solution to 0.8mL of 0.1M PBS solution.

Chapter 3

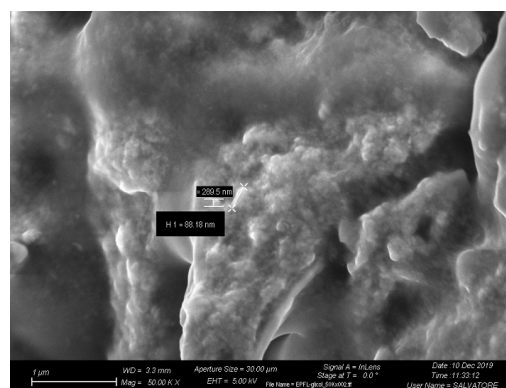
Results and Discussions

3.1 Characterization of Materials

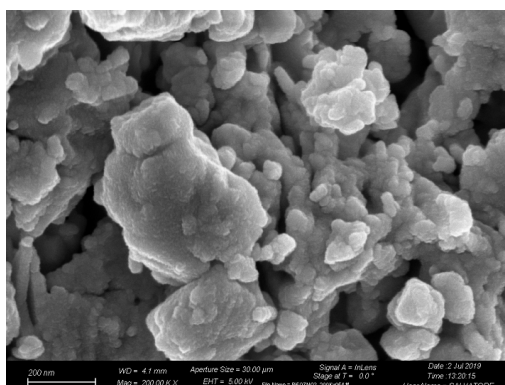
Field Emission Scanning Electron Microscopic (FE-SEM) experiments have been performed to identify the size, shape, and distribution of synthesized materials.



(a)



(b)



(c)

Figure 3.1: SEM images of (a) HO-BiONO₃ material with a magnification of 10K ×, (b) PEG-coated HO-BiONO₃ material with a magnification of 50K ×, and (c) Bi₅O₇NO₃ material with a magnification of 200K ×.

The figure 3.1a shows 1 μm scale SEM image of HO-BiONO₃ particles. It can be observed that the particles are distributed with a rod-shaped structure with dimensions in the submicron scale ($>100\text{nm}$). The figure 3.1b shows 1 μm scale SEM image of PEG-coated HO-BiONO₃ particles and the figure also shows a particle's estimated length and height. The SEM image of Bi₅O₇NO₃ is shown in figure 3.1c with 200nm scale. Observe the formation of aggregates with sphere-like nanoparticles of Bi₅O₇NO₃.

3.2 Surface characterization of SPEs

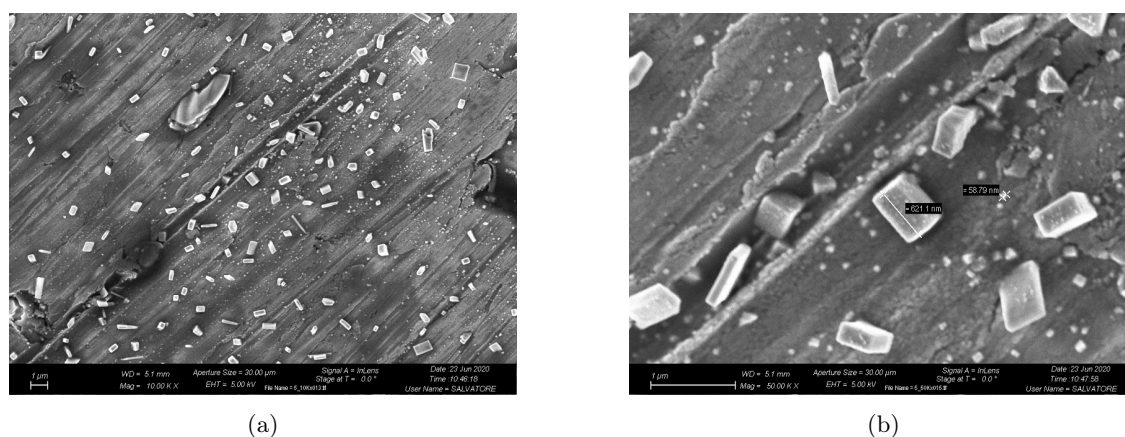


Figure 3.2: Scanning electron micrograph of (a) the working surface of HO-BiONO₃ modified SPE with a magnification of 10k \times and (b) The details of HO-BiONO₃ particles in 50k \times .

The distribution of HO-BiONO₃ particles on the surface of working electrode is shown in figure 3.2a and figure 3.2b shows the closer view of the same distribution. It can be noticed that the synthesized rod-shaped particles got broken into rectanguloid and cubic shaped particles with smaller sizes with uniform distribution.

Figures 3.3a and 3.3b show the distribution of PEG-coated HO-BiONO₃ and closer view of the distribution. Cubic shaped particles with different sizes can be observed and look like most of the particles got stabilized by PEG coating. The surface of the PEG-coated HO-BiONO₃ modified working electrode cleaned in 0.2M H₂SO₄ is shown in figures 3.3c and 3.3d. Figure 3.3d shows a very high density of particles with the same scale when compared to the distribution in figure 3.3b. Also, the formation of aggregates by breaking the particles into even smaller sized particles with cubic and rectanguloid shapes as we notice in the figure 3.3d.

Figure 3.4 shows the distribution of Bi₅O₇NO₃ particles on the working electrode surface of SPE. The distribution is uniform with different shapes and sizes of the Bi₅O₇NO₃ particles with a lower aggregation of particles compared to the synthesized material.

Figures 3.5a and 3.5b show the HO-BiONO₃ 5% wt coated Bi³⁺/Biochar particles distribution on the surface of working electrode. The same cubic shaped particles with different sizes can be noticed with uniform distribution all over the surface. But when it comes to the distribution of Bi₅O₇NO₃ 5% wt coated Bi³⁺/Biochar particles (figures 3.5c and 3.5d), the surface looks completely different when compared to the other modified working electrode surfaces as seen before with very small particles with different sizes.

For rectanguloid and cubic shaped particles the main electrochemical activity could be coming from their edges and corners of the particles. The size and distribution of different materials used to modify the electrode surfaces play a significant role in the determination of target molecules.

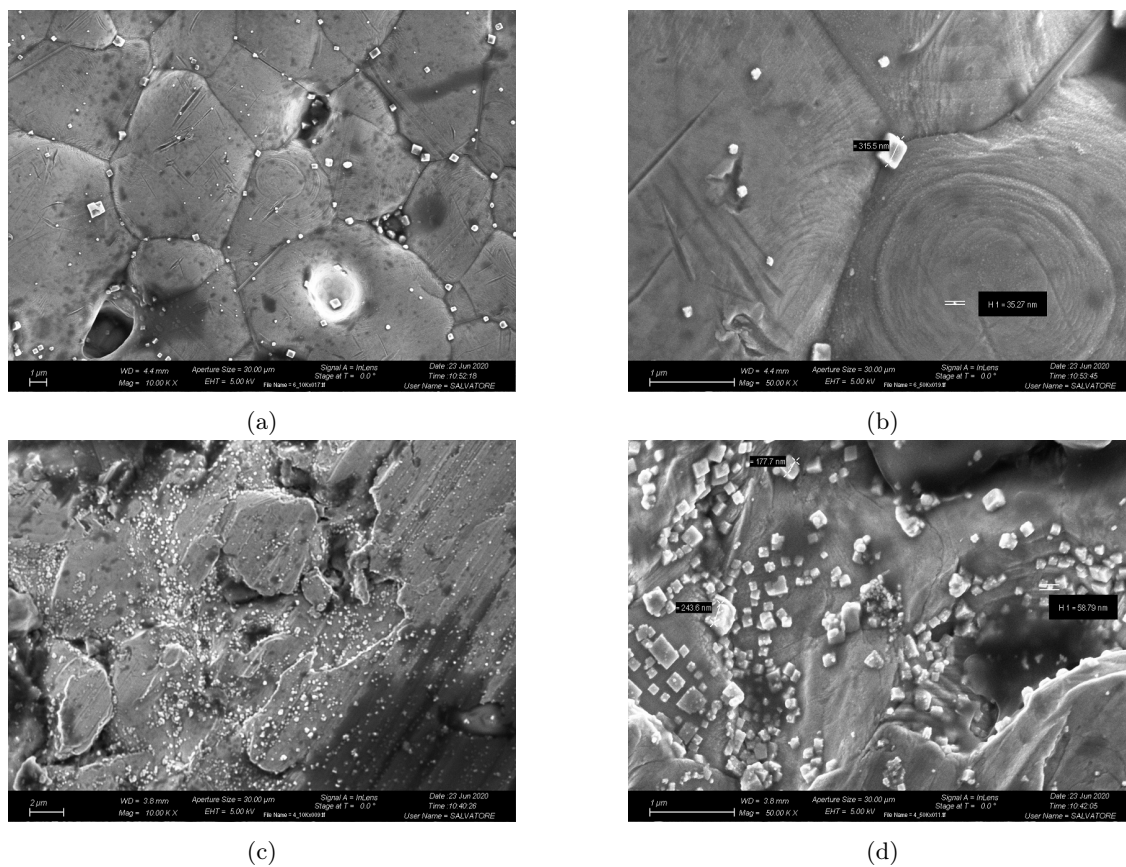


Figure 3.3: Scanning electron micrograph of (a) the working surface of PEG-coated HO-BiONO₃ modified SPE with a magnification of 10k ×, (b) details with a magnification of 50k ×, (c) working surface of PEG-coated HO-BiONO₃ modified SPE cleaned in 0.2M H₂SO₄ with a magnification of 10k ×, and (d) details with a magnification of 50k ×.

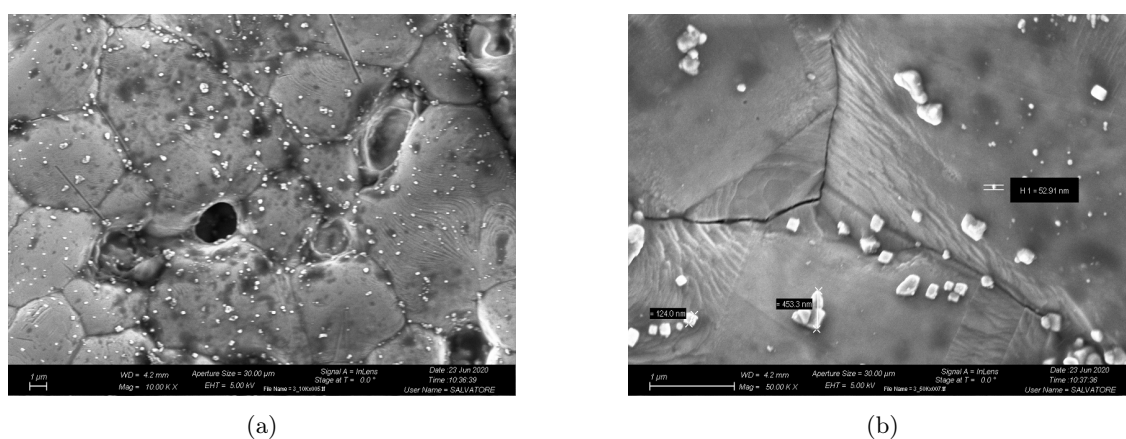


Figure 3.4: Scanning electron micrograph of (a) the working surface of Bi₅O₇NO₃ modified SPE with a magnification of 10k × and (b) details with a magnification of 50k ×.

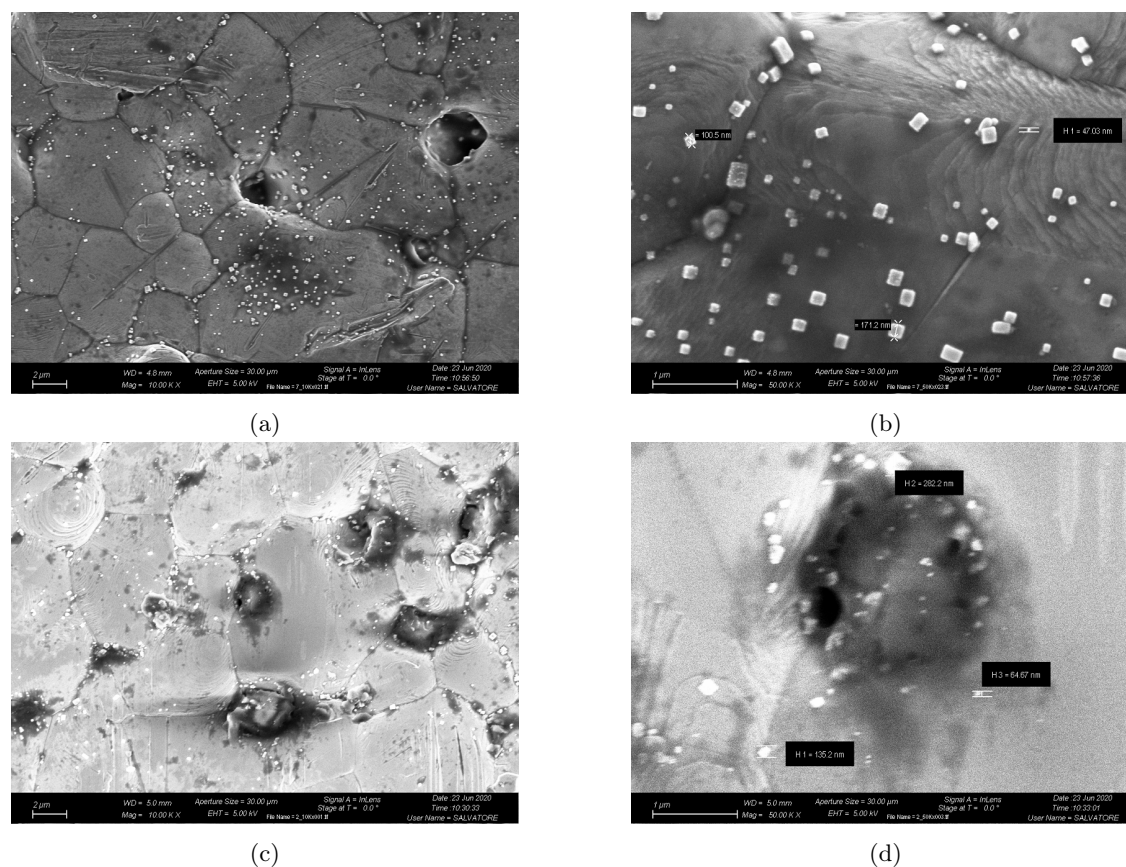


Figure 3.5: Scanning electron micrograph of (a) the working surface of HO-BiONO₃ 5% wt coated Bi³⁺/Biochar modified SPE with a magnification of 10k ×, (b) details with a magnification of 50k ×, (c) working surface of Bi₅O₇NO₃ 5% wt coated Bi³⁺/Biochar modified SPE with a magnification of 10k ×, and (d) details with a magnification of 50k ×.

3.3 Electrochemical Measurements

3.3.1 HO-BiONO₃ and Bi₅O₇NO₃ modified electrodes

The electrochemical performance of treated or modified screen-printed carbon electrodes (SPCEs) was studied by cyclic voltammetric (CV) experiments to determine 1mM paracetamol in 0.1M PBS at pH 7 by using Metrohm Autolab instrument in Potentiostatic mode. The cyclic voltammetric experiment was done by dropping 100 μL of the electrolytic solution on the surface of SPCE. The applied potential was ranging from -0.4 V to 0.8 V between the reference electrode and working electrode at a scan rate of 100 mV/s, and the current response was observed between working and counter electrodes. Figure 3.6a shows cyclic voltammograms of 0.1M PBS pH 7 and 1mM paracetamol in 0.1M PBS pH 7 when measured with unmodified SPCE. No peaks are observed with the voltage scan when there was no analyte in buffer solution (blue line) in figure 3.6a and there are clear peaks with anodic (Oxidation) and cathodic (Reduction) potential scans when there was an analyte in the buffer solution (red line).

Observed oxidation peak current of 33.1 ± 1.5 at peak potential 459.93 ± 0.98 which are measured after baseline correction of the plot shown in 3.6a. Then different SPC electrodes were modified by depositing 5μL, 10μL, 25μL, and 50μL of HO-BiONO₃ in steps of 5μL on the surface of the working electrode and the electrodes were used to measure cyclic voltammograms. It was found that the

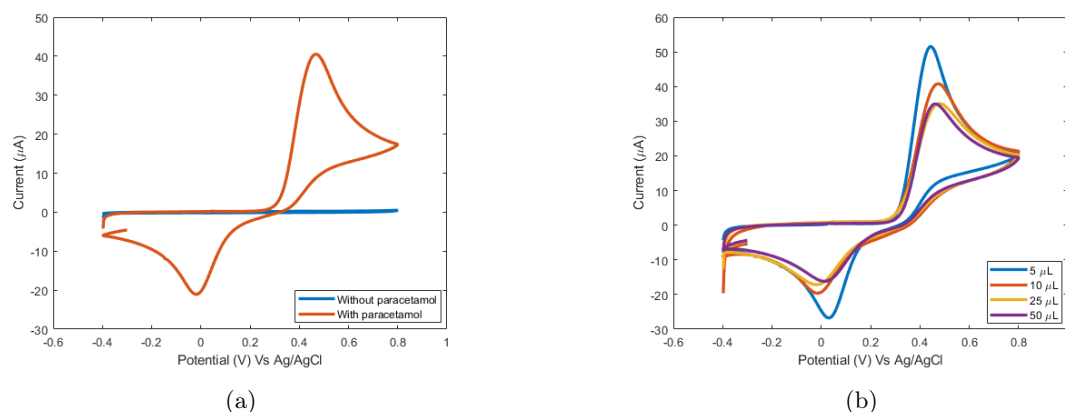


Figure 3.6: Cyclic voltammograms of 1 mM paracetamol in 0.1M PBS pH 7 at a scan rate of 100 mV/s with a) unmodified (bare) and b) HO-BiONO₃ modified electrodes with different amounts of deposition (shown in legend).

current response was decreasing with the increase in the amount of deposition as shown in figure 3.6b, which describes that thicker layer of BiONO₃ was affecting the electrical conductivity. Hence, 5 μL was fixed in this whole work in order to deposit on all electrodes for direct comparison. CVs for 5 μL HO-BiONO₃ deposited SPCE are compared with bare electrode measurements and reported in figure 3.7. Observed a small peak when there was no analyte (blue line) and clear oxidation and reduction peaks with the presence of the analyte (red line). Improvement in oxidation peak current (43.08 ± 0.80) and a negative shift in peak potential (434.0 ± 4.5) compared to the bare electrode can be observed.

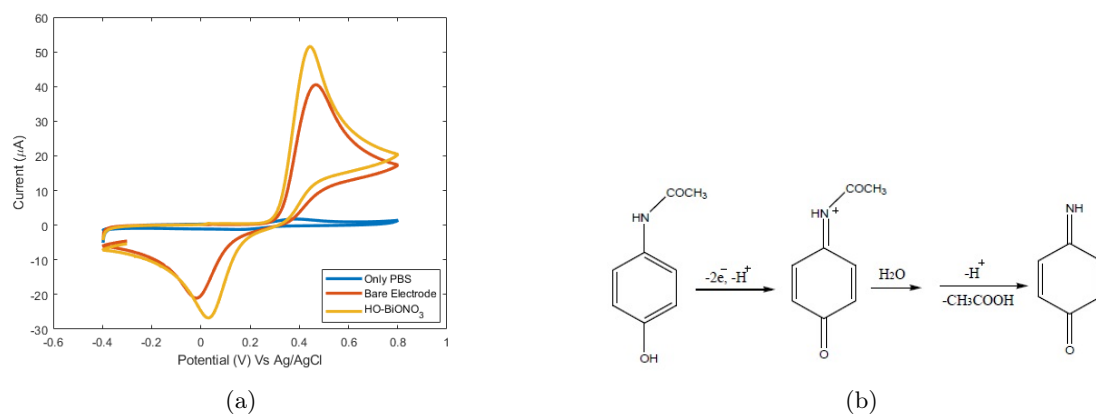


Figure 3.7: Cyclic voltammograms of 1 mM paracetamol in 0.1M PBS pH 7 at a scan rate of 100 mV/s with HO-BiONO₃ modified electrode and unmodified (bare) electrode. b) Possible oxidation mechanism of paracetamol [30].

Redox currents are due to the presence of paracetamol in PBS buffer solution that oxidizes with an anodic potential scan and reduces with cathodic potential scan. The redox mechanism of paracetamol is a two-electron and two proton process shown in figure 3.7b[19].

After the successful experiment using HO-BiONO₃ modified SPE, the investigation moved to modify the electrodes by depositing 5 μL of all other synthesized Bismuth composites. Using those modified electrodes cyclic voltammetric experiments were performed and observed that all the

modified electrodes resulted in higher oxidation and reduction peak currents and low redox potentials compared to the bare electrode when determining 1mM paracetamol in 0.1M PBS at pH 7. Cyclic voltammograms for modified electrodes and the bare electrode are shown in figure 3.8, indicating different materials used to modify the surface of the electrodes in the legend of each plot.

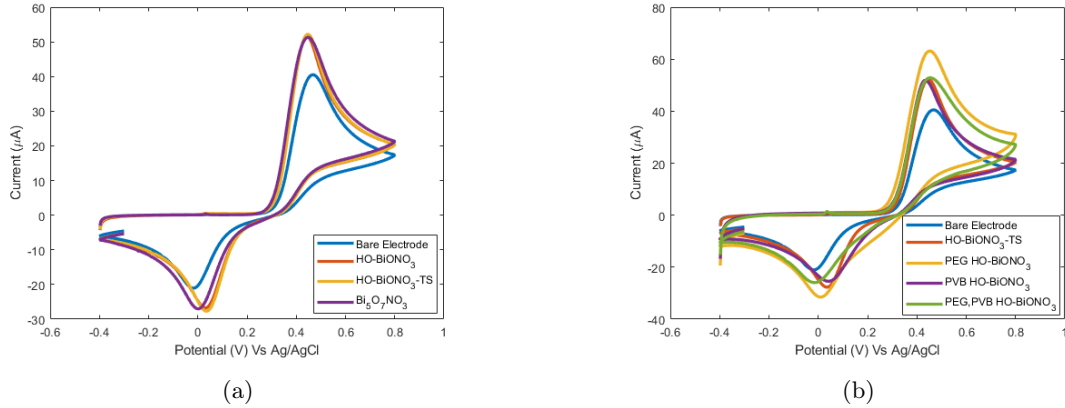


Figure 3.8: Cyclic voltammograms of 1 mM paracetamol in 0.1M PBS pH 7 at a scan rate of 100 mV/s with (a) $\text{Bi}_5\text{O}_7\text{NO}_3$, HO-BiONO₃ without surfactans modified and unmodified (bare) electrodes and (b) HO-BiONO₃ with and without surfactants modified and bare electrodes.

Table 3.1 shows the oxidation peak currents and corresponding anodic peak potentials with modified and bare electrodes. All values are shown with their respective standard deviations.

Material	Potential (mV)	Current (μA)
Bare Electrode	459.93 ± 0.98	33.1 ± 1.5
HO-BiONO ₃	434.0 ± 4.5	43.08 ± 0.80
HO-BiONO ₃ - TS	433.6 ± 6.1	42.0 ± 1.5
PEG-coated HO-BiONO ₃	385 ± 30	52.1 ± 3.0
PVB-coated HO-BiONO ₃	443 ± 19	40.9 ± 4.9
PEG & PVB-coated HO-BiONO ₃	403 ± 21	44.5 ± 1.3
$\text{Bi}_5\text{O}_7\text{NO}_3$	442.8 ± 3.9	43.0 ± 1.1

Table 3.1: Oxidation peak potentials and corresponding peak currents for different bare and modified electrodes.

As we notice the table 3.1 carefully, PEG-coated BiONO₃ modified electrode has given a higher oxidation peak current and a higher negative shift in overpotential compared to all other modified electrodes. Thanks to PEG which provides stability to most of the particles and stops from forming flocs or coagulates and also increases the active surface area of nanoparticles this has to be studied extensively [61]. PVB-coated BiONO₃ resulted in lower oxidation peak current and high peak potential among all the modified electrodes. In general, the PVB is a plasticizer, provides the good binding ability and optical clarity. PEG and PVB-coated BiONO₃ modified electrode has peak current and potential values which are like optimized values between PEG-coated and PVB-coated BiONO₃ modified electrodes. The reason could be that PVB provides a good binding ability to BiONO₃ particles which helps in an easy coating of PEG to provide stability to particles. $\text{Bi}_5\text{O}_7\text{NO}_3$ modified electrode also has a good improvement in both peak current and potential compared to the bare electrode. In general, it acts as a good photocatalyst due to its narrow bandgap.

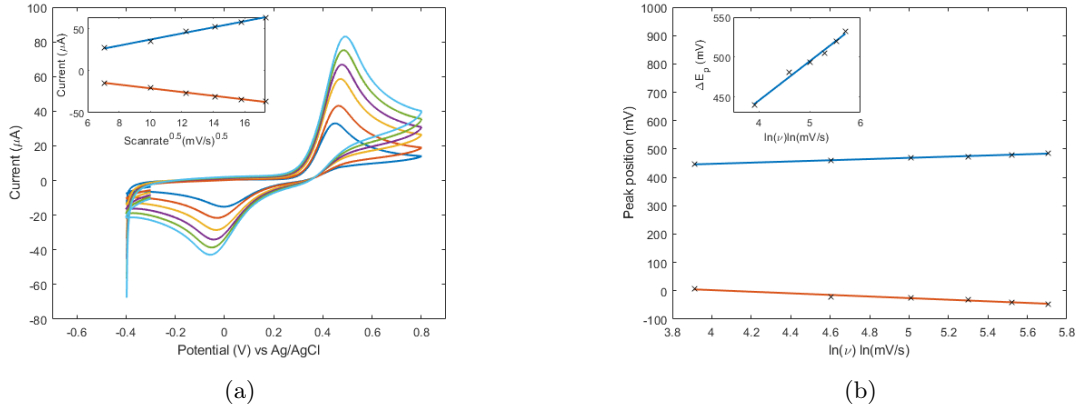


Figure 3.9: Bare electrode : (a) Cyclic voltammograms of 1 mM paracetamol in 0.1M PBS pH 7 with different scan rates (50, 100, 150, 200, 250, and 300 mV/s), inset: redox peak currents with square root of scan rate, (b) redox peak positions with $\ln(\nu)$ inset: peak-to-peak separation (ΔE_p) with $\ln(\nu)$.

To study the behavior of electrochemical system cyclic voltammetry was performed by varying the scan rate. Measurements were performed with the scan rate ranging from 50mV/s to 300mV/s in steps of 50mV/s to measure 1mM paracetamol in 0.1M PBS at pH 7. Figure 3.9a shows the cyclic voltammograms with the scan rate and redox peak positions with $\ln(\nu)$ measured with the bare electrode. The same are shown in figure 3.10 for HO-BiONO₃ modified electrode and PEG-coated HO-BiONO₃ modified electrode. The experiment was done for all the electrodes but only some are shown here for simplicity.

As we observe cyclic voltammograms with the scan rate, peak currents are increasing as the scan rate increases as shown in figures 3.9, 3.10, and also increasing linearly with the square root of scan rate as shown in inset figures. Linear regression current equations and their respective regression coefficients R^2 for bare and modified electrodes with different materials are shown in table 3.2. These observations conclude that the system involves freely diffusing redox species as discussed in chapter 1. Also, peak positions are shifting with the scan rate and the ratio between oxidation and reduction peak currents is not equal to 1. From all these observations it is possible to conclude that electrochemical systems are freely diffusing quasi-reversible systems. They can be used potentially in applications for amperometric detection.

Material	$I_{pa}(\mu A)$	R^2	$I_{pc}(\mu A)$	R^2
Bare Electrode	$3.64\sqrt{\nu}+0.83$	0.992	$-2.22\sqrt{\nu}+1.24$	0.994
HO-BiONO ₃	$4.01\sqrt{\nu}+3.07$	0.999	$-2.61\sqrt{\nu}+0.72$	0.998
HO-BiONO ₃ - TS	$3.96\sqrt{\nu}+1.98$	0.999	$-2.48\sqrt{\nu}+0.51$	0.997
PEG-coated HO-BiONO ₃	$6.21\sqrt{\nu}-10.76$	0.991	$-2.83\sqrt{\nu}-0.30$	0.990
PVB-coated HO-BiONO ₃	$3.78\sqrt{\nu}+ 2.84$	0.999	$-2.49\sqrt{\nu}-0.45$	0.999
PEG & PVB-coated HO-BiONO ₃	$4.36\sqrt{\nu}+ 1.14$	0.998	$-2.69\sqrt{\nu}-0.71$	0.999
Bi ₅ O ₇ NO ₃	$3.98\sqrt{\nu}+ 2.0$	0.999	$-2.57\sqrt{\nu}+0.34$	0.999

Table 3.2: Linear regression current equations with square root of scan rate and regression coefficients (R^2).

By extracting the anodic and cathodic peak positions for different scan rates for each electrode plotted with natural logarithm (\ln) of scan rate. Linear regression peak potential equations with

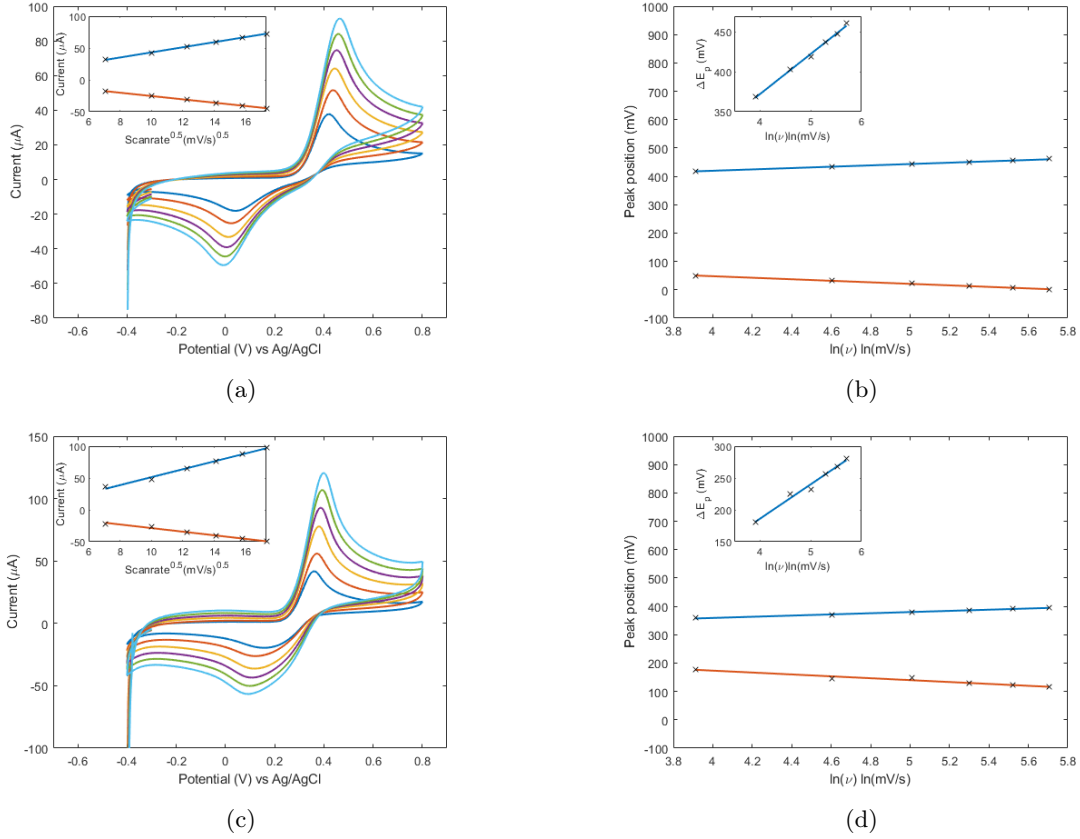


Figure 3.10: HO-BiONO₃ modified electrode : (a) Cyclic voltammograms of 1 mM paracetamol in 0.1M PBS pH 7 with different scan rates (50, 100, 150, 200, 250, and 300 mV/s), inset: redox peak currents with square root of scan rate, (b) redox peak positions with ln(scan rate) inset: peak-to-peak separation (ΔE_p) with ln(scan rate). PEG-coated HO-BiONO₃ modified electrode : (c) Cyclic voltammograms of 1 mM paracetamol in 0.1M PBS pH 7 with different scan rates (50, 100, 150, 200, 250, and 300 mV/s), inset: redox peak currents with square root of scan rate, (d) redox peak positions with ln(scan rate) inset: peak-to-peak separation (ΔE_p) with ln(scan rate).

$\ln(\nu)$ and respective regression coefficient (R) for each electrode are shown in table 3.3.

Material	E_{pa} (mV)	R	E_{pc} (mV)	R
Bare Electrode	$21.20\ln(\nu)+362.79$	0.995	$-28.22\ln(\nu)+115.34$	0.981
HO-BiONO ₃	$23.70\ln(\nu)+324.97$	0.997	$-26.88\ln(\nu)+155.41$	0.998
HO-BiONO ₃ - TS	$22.35\ln(\nu)+330.39$	0.993	$-29.89\ln(\nu)+165.61$	0.996
PEG-coated HO-BiONO ₃	$20.78\ln(\nu)+276.01$	0.993	$-33.41\ln(\nu)+306.97$	0.973
PVB-coated HO-BiONO ₃	$17.92\ln(\nu)+353.92$	0.996	$-24.11\ln(\nu)+151.74$	0.974
PEG & PVB-coated HO-BiONO ₃	$19.57\ln(\nu)+302.48$	0.990	$-31.99\ln(\nu)+241.30$	0.996
Bi ₅ O ₇ NO ₃	$19.97\ln(\nu)+350.14$	0.989	$-27.45\ln(\nu)+145.65$	0.987

Table 3.3: Linear regression peak potential equations with $\ln(\nu)$ and regression coefficient (R).

From the slopes of linear regression peak potential equations, it is possible to calculate the electron transfer coefficient (α) and electron transfer number (n) by equaling slope of cathodic peak positions line to $-2.3RT/\alpha nF$ and slope of anodic peak positions line to $2.3RT/(1-\alpha)nF$. Also,

half potentials ($E_{1/2}$) were calculated at a scan rate of 100 mV/s by using the formula

$$E_{1/2} = \frac{E_{pa} + E_{pc}}{2}. \quad (3.1)$$

All calculated values of α , n and $E_{1/2}$ are reported in table 3.4. Electron transfer number (n) is matching with the number of electrons involved in the redox mechanism of paracetamol. Also observe that PEG-coated HO-BiONO₃, PEG and PVB-coated HO-BiONO₃, and Bi₅O₇NO₃ modified electrodes have lower electron transfer coefficients (α) of 0.38, 0.38, and 0.42 respectively compared to bare electrode value of 0.43. Since only one data set available for CVs with scan rate hence, 95% confidence interval bound values (upper and lower bounds) were calculated in Matlab using `confint()` function for peak positions with $\ln(\nu)$. Figure 3.11 shows the estimated 95% confidence interval bound values for peak potentials for HO-BiONO₃, PEG-coated BiONO₃ modified electrodes only but this estimation was performed for all modified electrodes.

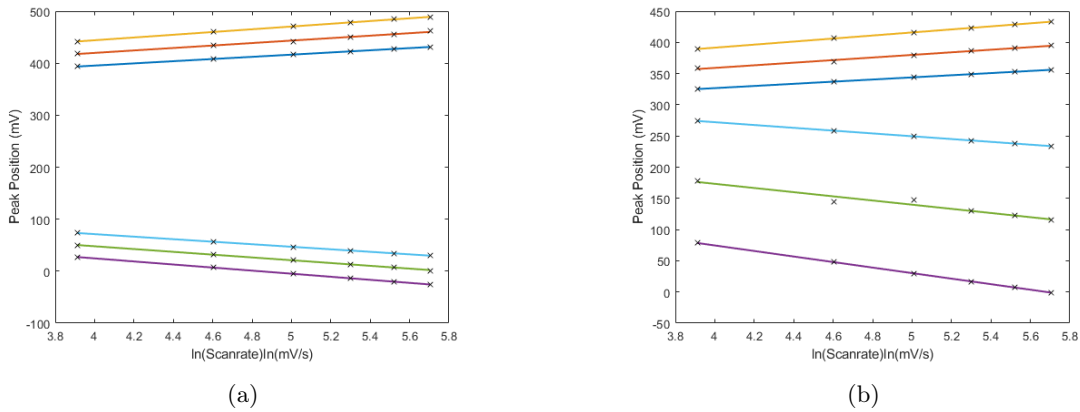


Figure 3.11: 95% confidence interval bound values (upper and lower bounds) for the peak potentials with $\ln(\nu)$ for (a) HO-BiONO₃ (b) PEG-coated HO-BiONO₃ modified electrodes where purple, green, and cyan colored solid lines represent the fitted lines for cathodic lower bound, experimental, and upper bound potentials respectively and blue, red, and yellow colored solid lines represent the fitted lines for anodic lower bound, experimental, and upper bound potentials respectively.

Different α values were calculated from the slopes of estimated lower and upper bound lines and also with the experimental data. The standard deviation was calculated for three values and reported with the experimental values in the table 3.4. The standard deviation for $E_{1/2}$ was also calculated in the same way with estimated bound values and reported with the experimental value.

Material	$E_{1/2}$ (mV)	Alpha (α)	n
Bare Electrode	221 ± 52	0.44 ± 0.10	2
HO-BiONO ₃	233 ± 25	0.468 ± 0.052	2
HO-BiONO ₃ - TS	231 ± 34	0.428 ± 0.068	2
PEG-coated HO-BiONO ₃	260 ± 70	0.39 ± 0.12	2
PVB-coated HO-BiONO ₃	238 ± 49	0.44 ± 0.11	2
PEG & PVB-coated HO-BiONO ₃	242 ± 37	0.380 ± 0.074	2
Bi ₅ O ₇ NO ₃	230 ± 50	0.42 ± 0.10	2

Table 3.4: Half potential ($E_{1/2}$) at a scan rate of 100 mV/s, electron transfer coefficient (α) and electron transfer number (n).

Peak-to-peak separation (ΔE_p) at 100 mV/s with standard deviations are reported in table 3.5, calculated as described above with estimated bound values and also respective linear regression equations with $\ln(\nu)$ for modified and unmodified electrodes. Observe that peak-to-peak separation is increasing linearly with $\ln(\nu)$ as shown in figure 3.10. PEG-coated BiONO₃ modified electrode has a ΔE_p of 221 mV which is lesser compared to other electrodes and is 256 mV less than the unmodified electrode. This means that this electrode has a more possible reversible reaction and also less resistance compared to other electrodes since ΔE_p is directly related to the kinetics of electron transfer. This electrode can also provide faster electron transfer reactions compared to other electrodes. An uncompensated resistance can be observed with a change in concentration of analyte which increases ΔE_p with concentration as observed in figure 3.12. With the help of ΔE_p approximate kinetic parameters can be evaluated to compare the performance among electrodes.

Material	ΔE_p (mV)	R	ΔE_p (mV)
Bare Electrode	$49.42\ln(\nu)+247.46$	0.994	477 ± 45
HO-BiONO ₃	$50.58\ln(\nu)+169.56$	0.998	402.6 ± 1.1
HO-BiONO ₃ - TS	$52.24\ln(\nu)+164.77$	0.997	405.30 ± 0.95
PEG-coated HO-BiONO ₃	$54.20\ln(\nu)-30.96$	0.991	221 ± 71
PVB-coated HO-BiONO ₃	$42.03\ln(\nu)+202.18$	0.992	398 ± 52
PEG & PVB-coated HO-BiONO ₃	$51.57\ln(\nu)+61.19$	0.995	298.40 ± 0.51
Bi ₅ O ₇ NO ₃	$47.42\ln(\nu)+204.48$	0.992	423 ± 20

Table 3.5: Linear regression peak-peak separation (ΔE_p) equations with $\ln(\nu)$ and regression coefficient (R). ΔE_p values at a scan rate of 100 mV/s with standard deviations.

From the Laviron model discussed in chapter 1, as we see the $n\Delta E_p$ is greater than 200 mV, it is possible to apply the first condition of Laviron model [15] in order to calculate the rate constant (k). The kinetic rate constant (k) was calculated using the equation 1.20 for all electrodes at a scan rate of 100 mV/s and listed in table 3.6 with standard deviations calculated by using the bound values. One can observe in the table that the standard deviation is higher than the experimental value for some electrodes since the equation 1.20 is not a linear equation in α and ΔE_p . Though α is lower, due to low ΔE_p PEG-coated BiONO₃ modified electrode has a higher k value of 58.2 ms⁻¹ as discussed above, meaning that this involves in faster electron transfer reaction compared to other electrodes and also it has low over potential among other electrodes.

Material	k (ms ⁻¹)	D (cm ² /s)
Bare Electrode	0.60 ± 0.33	1.48×10^{-6}
HO-BiONO ₃	1.70 ± 0.20	2.21×10^{-6}
HO-BiONO ₃ - TS	1.90 ± 0.54	2.00×10^{-6}
PEG-coated HO-BiONO ₃	$58.2 \pm 1.0 \times 10^2$	2.70×10^{-6}
PVB-coated HO-BiONO ₃	2.9 ± 2.1	2.01×10^{-6}
PEG & PVB-coated HO-BiONO ₃	16.8 ± 5.2	2.28×10^{-6}
Bi ₅ O ₇ NO ₃	1.60 ± 0.26	2.11×10^{-6}

Table 3.6: Rate constant (k) and diffusion coefficient (D) of paracetamol at a scan rate of 100 mV/s for bare and modified electrodes.

Diffusion coefficient (D) was also calculated using equation 1.15 at 100 mV/s scan rate by taking the geometrical area (A) of the working electrode equal to 0.12 cm². Diffusion coefficients for bare and modified electrodes at 100 mV/s scan rate are reported in table 3.6. All modified electrodes have higher diffusion coefficients compared to the unmodified electrode which has a D value of 1.48×10^{-6} cm²/s. PEG-coated BiONO₃ modified electrode has higher diffusion coefficient of 2.70×10^{-6} cm²/s compared to other electrodes.

Calibration Curves

For any electrochemical system, these factors such as stability, repeatability, reproducibility, and sensitivity are very important to assess its application in sensing and control processes. Paracetamol was quantified by CV at a scan rate of 100 mV/s by measuring oxidation peak currents. The oxidation peak currents have shown a linear relationship with concentration ranging from 0.5 mM to 3 mM, linear regression equations of oxidation current for bare and modified electrodes are shown in table 3.7. Cyclic voltammograms of paracetamol in 0.1M PBS at pH 7 by varying the concentration of paracetamol for HO-BiONO₃ and PEG-coated HO-BiONO₃ modified electrodes are shown in figure 3.12. It can be observed that redox peak currents are increasing with concentration and ΔE_p is increasing due to uncompensated resistance.

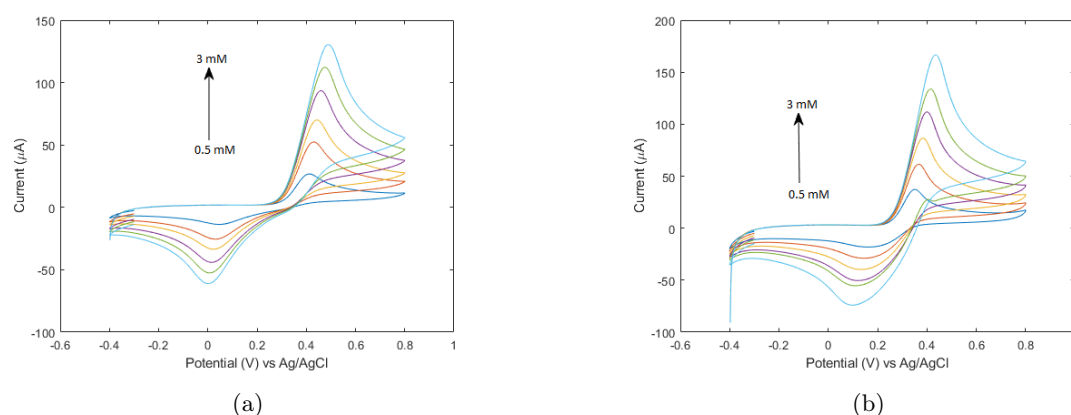


Figure 3.12: Cyclic voltammograms of 0.5 mM to 3 mM paracetamol in 0.1M PBS pH 7 with (a) HO-BiONO₃ and (b) PEG-coated HO-BiONO₃ modified electrodes.

Material	I_p (μA)	R^2 (n=3)
Bare Electrode	20.02[C]+8.77	0.994
HO-BiONO ₃	32.77[C]+8.56	0.995
HO-BiONO ₃ - TS	34.88[C]+6.12	0.996
PEG-coated HO-BiONO ₃	43.50[C]+ 11.08	0.998
PVB-coated HO-BiONO ₃	32.35[C]+9.41	0.995
PEG & PVB-coated HO-BiONO ₃	36.51[C]+8.55	0.996
Bi ₅ O ₇ NO ₃	35.86[C]+7.26	0.991

Table 3.7: Linear regression equations of oxidation peak current with concentration (C) of analyte and their regression coefficients (R^2).

Three calibration curves were acquired for paracetamol from 0.5mM to 3mM concentration range in steps of 0.5mM in order to check the repeatability of the system. Electrodes were cleaned with distilled water before dispensing successive sample drops with different concentrations and voltammetric analysis time for each concentration of paracetamol was 30s. Calibration curves were plotted by taking oxidation peak currents for each concentration. The average of three calibration curves and standard deviation of their slopes was calculated for bare and all modified electrodes. Calibration curves for bare and modified electrodes are shown in figure 3.13 with their standard deviations indicated as error bars.

Sensitivity (S) of each electrode was obtained by taking into account the slope of the respective

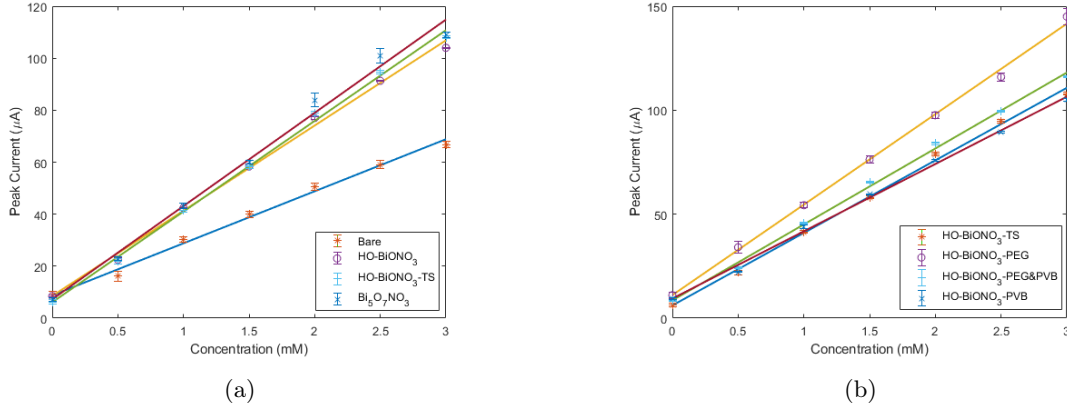


Figure 3.13: Calibration curves for different electrodes indicated in legends of (a) and (b).

Material	Sensitivity ($\mu\text{A}/\text{mM}$)	LOD (μM)	R.S.D(n=3)
Bare Electrode	20.02 ± 0.23	2.316 ± 0.026	1.15%
HO-BiONO ₃	32.77 ± 0.25	7.159 ± 0.054	0.76%
HO-BiONO ₃ - TS	34.88 ± 0.15	2.793 ± 0.012	0.48%
PEG-coated HO-BiONO ₃	43.50 ± 0.54	2.235 ± 0.028	1.24%
PVB-coated HO-BiONO ₃	32.35 ± 0.42	3.716 ± 0.039	1.29%
PEG & PVB-coated HO-BiONO ₃	36.511 ± 0.011	1.48763 ± 0.00037	0.03%
Bi ₅ O ₇ NO ₃	35.86 ± 0.64	5.683 ± 0.083	1.78%

Table 3.8: Sensitivity and Limit of detection (LOD) for bare and HO-BiONO₃ and Bi₅O₇NO₃ modified electrodes with their relative standard deviations (R.S.D).

calibration curve. Limit of detection (LOD) was calculated by using the formula

$$LOD = \frac{KD}{S}. \quad (3.2)$$

Where K is statistical confidence level 1 for 68.2% , 2 for 95.4%, and 3 for 99.6%, D is the standard deviation of blank measurements and S is the sensitivity[11, 58].

All the sensitivities and limits of detection values with their standard deviations and relative standard deviations (R.S.D) of electrodes are shown in table 3.8 for bare and modified electrodes. Bare electrode has a sensitivity of 20.02 ± 0.23 with LOD 2.316 ± 0.026 ($R^2 = 0.994$, $n=3$) and R.S.D of 1.15%. Among all the modified electrodes PEG-coated BiONO₃ modified electrode has a higher sensitivity of 43.50 ± 0.54 which is more than double of bare electrode sensitivity with LOD 2.235 ± 0.028 ($R^2=0.998$, $n=3$) and R.S.D of 1.24%. When it comes to limit of detection PEG & PVB-coated BiONO₃ modified electrode has a very low value of 1.48763 ± 0.00037 with sensitivity equal to 36.511 ± 0.011 ($R^2=0.996$, $n=3$) and R.S.D of 1.29%. Bi₅O₇NO₃ modified electrode also has a good sensitivity of 35.86 ± 0.64 ($R^2 =0.991$, $n=3$) with R.S.D of 1.78%. According to equation 3.2, the limit of detection has to decrease as the sensitivity increases but it's not happening as reported by the table 3.8 since it also depends on blank measurements and these electrodes behave differently for the blank solution.

3.3.2 Cyclic Voltammetry in H₂SO₄

Inspired by the work of Aoife Morrin et al [62], a new SPE was modified by depositing $5\mu\text{L}$ of PEG-coated HO-BiONO₃ and then performed cyclic voltammetry to determine 1mM paracetamol

in 0.1M PBS at pH 7. After that, the modified electrode was cleaned in deionized (DI) water and dried with N_2 air. After cleaning and drying, the electrode was dipped in 0.2M H_2SO_4 and performed one step of CV by applying a potential from -1.2V to 1.5V at a scan rate of 100 mV/s. Then electrode was dried with N_2 air to perform CV in determining paracetamol. This procedure of measuring paracetamol, cleaning and drying, CV in 0.2M H_2SO_4 , and then drying was performed repeatedly for 6 times on the same day. In the end, modified SPE was stored in DI water for further use.

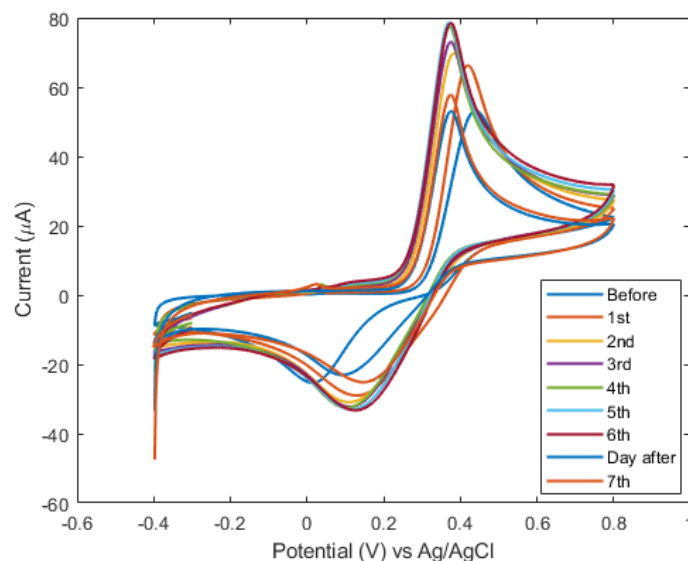


Figure 3.14: Cyclic voltammograms of 1mM paracetamol in 0.1M PBS pH 7 at a scan rate of 100 mV/s with PEG-coated HO-BiONO₃ modified electrode before and after each step of CV in 0.2M H_2SO_4 (Corresponding voltammogram after each step is indicated in legend).

# CV in H_2SO_4	Ox. Potential(mV)	Current(μA)	Re. Potential(mV)	Current(μA)
Before	437.37	45.19	22.43	-27.55
1	417.94	57.56	146.94	-33.19
2	381.32	59.95	129.85	-33.51
3	373.99	62.45	127.41	-34.40
4	371.55	66.40	117.65	-35.85
5	371.55	67.07	139.62	-34.24
6	373.99	65.91	144.50	-35.60
Following day	373.99	46.22	105.44	-23.90
7	373.99	49.95	161.59	-26.67

Table 3.9: Measured oxidation, reduction potentials and peak currents after CV in H_2SO_4 for PEG-coated HO-BiONO₃ modified electrode.

The following day, the same electrode was used to measure 1mM paracetamol in 0.1M PBS pH 7. Again cleaned, dried, and performed CV in H_2SO_4 then measured paracetamol again. All obtained cyclic voltammograms in determining paracetamol before and after each step of CV in 0.2M H_2SO_4 are shown in figure 3.14. From figure 3.14, it can be observed that after each step of CV in H_2SO_4 the oxidation current was increased and settled around 65 μA . Then oxidation current was registered as decreased the following day to 46.22 μA and again increased after a step

of CV in H_2SO_4 . Obtained oxidation, reduction peak currents, and respective peak positions are shown in table 3.9.

The effect was immediate just after CV in H_2SO_4 and it can be understood by doing an extensive study on the modified electrode surface before CV in H_2SO_4 and after CV in H_2SO_4 . There is a chance of change in pH since, H_2SO_4 is an acidic medium but the experiments were done by assuming that the medium is at pH 7, and also observed a clear change on the surface of the electrode with the naked eye after performing CV in H_2SO_4 . It is evident from figure 3.3d and H_2SO_4 broke the particles into even smaller sizes by the formation of aggregation of particles.

3.3.3 Bi^{3+} /Biochar modified electrodes

Bi^{3+} /Biochar composites modified SPCEs also used to determine 1mM paracetamol in 0.1M PBS at pH 7. Cyclic voltammograms for bare and modified electrodes are shown in figure 3.15 at a scan rate of 100 mV/s.

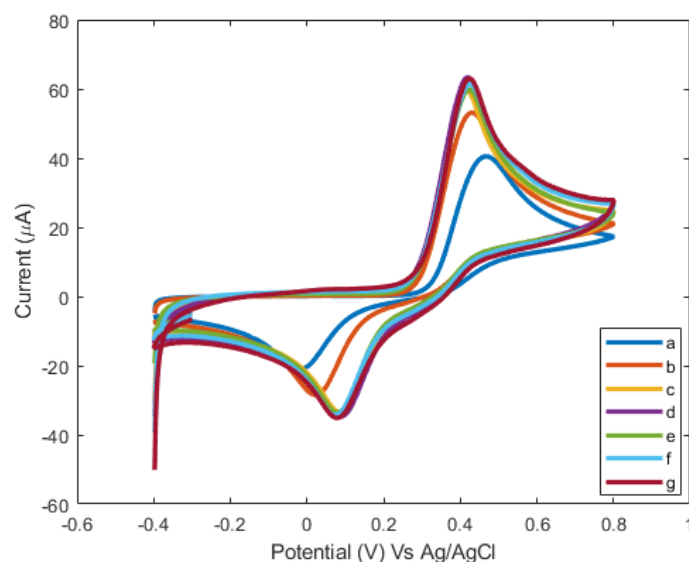


Figure 3.15: Cyclic voltammograms of 1 mM paracetamol in 0.1M PBS pH 7 at a scan rate of 100 mV/s with (a) unmodified, (b) HO-BiONO₃ 5% Wt Bi³⁺/Biochar, (c) HO-BiONO₃ 10% Wt Bi³⁺/Biochar, (d) HO-BiONO₃ 15% Wt Bi³⁺/Biochar, (e) Bi₅O₇NO₃ 5% Wt Bi³⁺/Biochar, (f) Bi₅O₇NO₃ 10% Wt Bi³⁺/Biochar, and (g) Bi₅O₇NO₃ 15% Wt Bi³⁺/Biochar modified electrodes.

Material	Potential (mV) \pm SD	Current (μA) \pm SD
HO-BiONO ₃ 5% Wt Bi ³⁺ /Biochar	428 \pm 23	45.5 \pm 2.3
HO-BiONO ₃ 10% Wt Bi ³⁺ /Biochar	413 \pm 15	50.4 \pm 2.9
HO-BiONO ₃ 15% Wt Bi ³⁺ /Biochar	418 \pm 28	52.6 \pm 2.4
Bi ₅ O ₇ NO ₃ 5% Wt Bi ³⁺ /Biochar	420 \pm 31	50.7 \pm 3.3
Bi ₅ O ₇ NO ₃ 10% Wt Bi ³⁺ /Biochar	423 \pm 24	50.9 \pm 3.4
Bi ₅ O ₇ NO ₃ 15% Wt Bi ³⁺ /Biochar	420 \pm 26	51.4 \pm 3.7

Table 3.10: Oxidation peak potentials and corresponding peak currents for Bi³⁺/Biochar modified electrodes.

Bi³⁺/Biochar composites modified SPCEs showed a good promise compared to the bare electrode's

performance, the resulted peak positions and oxidation peak currents are shown in table 3.10. Among all the modified electrodes HO-BiONO₃ 15% Wt Bi³⁺/Biochar modified electrode resulted in an oxidation peak current of $52.6 \pm 2.4 \mu\text{A}$, and for Bi₅O₇NO₃ 15% Wt Bi³⁺/Biochar modified electrode returned an oxidation peak current of $51.4 \pm 3.7 \mu\text{A}$.

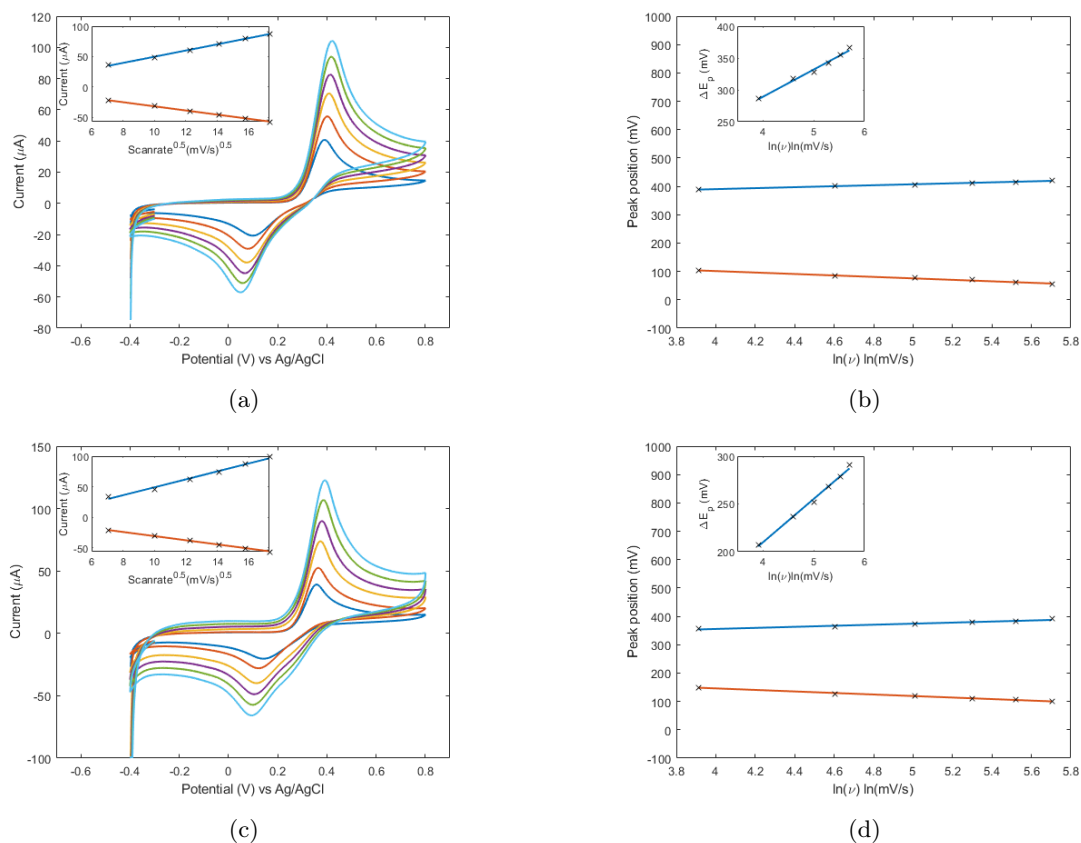


Figure 3.16: HO-BiONO₃ 5% Wt Bi³⁺/Biochar modified electrode: (a) Cyclic voltammograms of 1 mM paracetamol in 0.1M PBS pH 7 with different scan rates (50, 100, 150, 200, 250, and 300 mV/s), inset: redox peak currents with square root of scan rate, (b) redox peak positions with $\ln(\text{scan rate})$ inset: ΔE_p with $\ln(\text{scan rate})$. Bi₅O₇NO₃ 5% Wt Bi³⁺/Biochar modified electrode: (c) Cyclic voltammograms of 1 mM paracetamol in 0.1M PBS pH 7 with same scan rates (50, 100, 150, 200, 250, and 300 mV/s), inset: redox peak currents with square root of scan rate, (d) redox peak positions with $\ln(\text{scan rate})$ inset: ΔE_p with $\ln(\text{scan rate})$.

Similarly as in the previous case of modified electrodes, cyclic voltammetry was performed by varying the scan rate from 50 mV/s to 300 mV/s in steps of 50 mV/s. Resulted cyclic voltammograms for HO-BiONO₃ 5% Wt Bi³⁺/Biochar modified electrode and Bi₅O₇NO₃ 5% Wt Bi³⁺/Biochar modified electrodes are shown in 3.16. The figure also shows the variation of peak positions with respect to the natural logarithm of scan rate and peak-to-peak separation (ΔE_p) with $\ln(\text{scan rate})$. Cyclic voltammograms with scan rate were measured for all six modified electrodes but only for two electrodes is shown in the figure for simplicity.

As well as in the previous case, peak positions varying with scan rate and peak currents varying linearly with the square root of scan rate as shown in inset figures of figure 3.16. Thus, we can conclude that electrochemical systems are freely diffusing quasi-reversible systems. Table 3.11 shows the linear regression current equations with respective regression coefficients (R^2). Can observe a good linear relationship for both oxidation and reduction peak currents for all electrodes.

Material	$I_{pa}(\mu A)$	R^2	$I_{pc}(\mu A)$	R^2
HO-BiONO ₃ 5% Wt Bi ³⁺ /Biochar	$5.11\sqrt{\nu}-1.37$	0.998	$-3.42\sqrt{\nu}+2.10$	0.998
HO-BiONO ₃ 10% Wt Bi ³⁺ /Biochar	$4.38\sqrt{\nu}+1.64$	0.999	$-2.92\sqrt{\nu}+0.31$	0.999
HO-BiONO ₃ 15% Wt Bi ³⁺ /Biochar	$6.37\sqrt{\nu}-11.54$	0.993	$-3.61\sqrt{\nu}+3.84$	0.996
Bi ₅ O ₇ NO ₃ 5% Wt Bi ³⁺ /Biochar	$6.49\sqrt{\nu}-15.71$	0.988	$-3.39\sqrt{\nu}+3.26$	0.996
Bi ₅ O ₇ NO ₃ 10% Wt Bi ³⁺ /Biochar	$8.19\sqrt{\nu}-31.15$	0.978	$-3.39\sqrt{\nu}+5.77$	0.959
Bi ₅ O ₇ NO ₃ 15% Wt Bi ³⁺ /Biochar	$6.36\sqrt{\nu}-16.01$	0.975	$-3.33\sqrt{\nu}+4.23$	0.998

Table 3.11: Linear regression peak current equations with square root of scan rate and regression coefficients (R^2) for Bi³⁺/Biochar modified electrodes.

Linear regression equations for peak potentials with $\ln(\nu)$ are also listed in table 3.12 with respective regression coefficients (R) and some of the plots are shown in figure 3.16. These showed a linear relationship with the natural logarithm of the scan rate as we observe the figures. Hence, calculated the half potentials $E_{1/2}$ by taking the mean of anodic and cathodic peak potentials at a scan rate 100 mV/s.

Material	$E_{pa}(mV)$	R	$E_{pc}(mV)$	R
HO-BiONO ₃ 5% Wt Bi ³⁺ /Biochar	$17.10\ln(\nu)+321.84$	0.997	$-25.78\ln(\nu)+204.46$	0.987
HO-BiONO ₃ 10% Wt Bi ³⁺ /Biochar	$22.96\ln(\nu)+297.18$	0.971	$-30.46\ln(\nu)+211.61$	0.985
HO-BiONO ₃ 15% Wt Bi ³⁺ /Biochar	$19.44\ln(\nu)+288.46$	0.981	$-27.97\ln(\nu)+242.68$	0.996
Bi ₅ O ₇ NO ₃ 5% Wt Bi ³⁺ /Biochar	$18.67\ln(\nu)+280.91$	0.976	$-26.87\ln(\nu)+253.45$	0.997
Bi ₅ O ₇ NO ₃ 10% Wt Bi ³⁺ /Biochar	$21.99\ln(\nu)+276.44$	0.993	$-22.12\ln(\nu)+223.97$	0.957
Bi ₅ O ₇ NO ₃ 15% Wt Bi ³⁺ /Biochar	$16.23\ln(\nu)+306.14$	0.987	$-22.77\ln(\nu)+216.22$	0.984

Table 3.12: Linear regression peak potential equations with square root of scan rate and regression coefficients (R) for Bi³⁺/Biochar modified electrodes.

Material	$E_{1/2}$ (mV)	Alpha (α)	n
HO-BiONO ₃ 5% Wt Bi ³⁺ /Biochar	243 ± 36	0.404 ± 0.079	2
HO-BiONO ₃ 10% Wt Bi ³⁺ /Biochar	237 ± 73	0.43 ± 0.14	2
HO-BiONO ₃ 15% Wt Bi ³⁺ /Biochar	246 ± 44	0.41 ± 0.10	2
Bi ₅ O ₇ NO ₃ 5% Wt Bi ³⁺ /Biochar	248 ± 42	0.41 ± 0.10	2
Bi ₅ O ₇ NO ₃ 10% Wt Bi ³⁺ /Biochar	248 ± 63	0.49 ± 0.15	2
Bi ₅ O ₇ NO ₃ 15% Wt Bi ³⁺ /Biochar	245 ± 45	0.42 ± 0.12	2

Table 3.13: Half potential $E_{1/2}$ at a scan rate of 100 mV/s, electron transfer coefficient (α) and electron transfer number (n) for Bi³⁺/Biochar modified electrodes.

Electron transfer coefficient (α) and electron transfer number (n) were calculated from the slopes of peak potential equations using the Laviron model like in previous cases. Calculated values of $E_{1/2}$ at 100 mV/s, α and n are reported in table 3.13. Electron transfer number is coherent with the value present in literature and every electrode has a different α value as we observe the table which is very well comparable or higher than the bare electrode coefficient of 0.43. The standard deviation of α was calculated by using 95% bound values of slopes from peak positions as done previously.

Peak-to-peak separation ΔE_p was calculated by taking the difference between anodic and cathodic peak potentials and was also plotted with $\ln(\nu)$. Observe that ΔE_p is varying linearly with $\ln(\nu)$ as shown in figures 3.16b and 3.16d. Linear regression equations of ΔE_p are listed in table 3.14 with respective regression coefficients. And also listed ΔE_p with their standard deviation calculated

from 95% bound values at a scan rate of 100 mV/s, figure 3.17 shows that ΔE_p is increasing with the concentration of paracetamol due to an uncompensated resistance as stated before.

Material	$\Delta E_p(\text{mV})$	R	$\Delta E_p(\text{mV})$
HO-BiONO ₃ 5% Wt Bi ³⁺ /Biochar	$42.88\ln(\nu)+117.38$	0.993	316 ± 40
HO-BiONO ₃ 10% Wt Bi ³⁺ /Biochar	$53.42\ln(\nu)+85.57$	0.981	327.7 ± 8.3
HO-BiONO ₃ 15% Wt Bi ³⁺ /Biochar	$47.41\ln(\nu)+45.78$	0.993	263 ± 17
Bi ₅ O ₇ NO ₃ 5% Wt Bi ³⁺ /Biochar	$45.54\ln(\nu)+27.46$	0.996	237 ± 29
Bi ₅ O ₇ NO ₃ 10% Wt Bi ³⁺ /Biochar	$44.12\ln(\nu)+52.47$	0.988	258 ± 54
Bi ₅ O ₇ NO ₃ 15% Wt Bi ³⁺ /Biochar	$38.99\ln(\nu)+89.92$	0.991	270 ± 21

Table 3.14: Linear regression equations of ΔE_p with $\ln(\nu)$ and ΔE_p at a scan rate of 100 mV/s for Bi³⁺/Biochar modified electrodes.

And finally, the rate constant (k) and diffusion coefficient of paracetamol (D) were calculated again by using the Laviron model and equation 1.15. Resulted values of k and D are reported in table 3.15 and it shows that Bi₅O₇NO₃ 5% Wt Bi³⁺/Biochar modified electrode has a higher rate constant of 43.6 (ms⁻¹) due to its lower ΔE_p of 236.8 mV at a scan rate of 100 mV/s compared to other electrodes. When it comes to diffusion coefficient (D), HO-BiONO₃ 15% Wt Bi³⁺/Biochar modified electrode has a D value of 2.94e-06, which is higher among all electrodes tested in this work.

Material	k (ms ⁻¹)	D (cm ² /s)
HO-BiONO ₃ 5% Wt Bi ³⁺ /Biochar	12.1 ± 6.0	2.87×10^{-6}
HO-BiONO ₃ 10% Wt Bi ³⁺ /Biochar	10.5 ± 5.2	2.60×10^{-6}
HO-BiONO ₃ 15% Wt Bi ³⁺ /Biochar	32 ± 18	2.94×10^{-6}
Bi ₅ O ₇ NO ₃ 5% Wt Bi ³⁺ /Biochar	44 ± 41	2.56×10^{-6}
Bi ₅ O ₇ NO ₃ 10% Wt Bi ³⁺ /Biochar	46 ± 48	2.57×10^{-6}
Bi ₅ O ₇ NO ₃ 15% Wt Bi ³⁺ /Biochar	26.7 ± 4.7	2.58×10^{-6}

Table 3.15: Rate constant (k) and diffusion coefficient (D) at a scan rate of 100 mV/s for Bi³⁺/Biochar modified electrodes.

To find the sensitivity of electrodes, CVs were measured three times by varying the concentration of paracetamol from 0.5mM to 3mM in steps of 0.5mM. Figure 3.17 shows CVs with concentration of paracetamol in 0.1M PBS at pH 7 for HO-BiONO₃ 5% Wt Bi³⁺/Biochar and Bi₅O₇NO₃ 15% Wt Bi³⁺/Biochar modified electrodes. But, in the case of HO-BiONO₃ 10% Wt Bi³⁺/Biochar, it was observed that an increment in oxidation current more than double of what was observed in initial measurements. Hence, a new electrode was modified again and then performed the measurements to construct calibration curves.

Calibration curves were obtained by taking the average of three oxidation peak currents at each concentration as shown in figure 3.17c for some of the Biochar modified electrodes as indicated in the legend of the figure. As we observe, the oxidation peak current showed good linearity with increasing concentration with linear regression equations and respective regression coefficients as reported in table 3.16.

Sensitivity of electrodes was calculated by taking the slope of constructed calibration curves for each electrode and the values are listed in table 3.17. HO-BiONO₃ 15% Wt Bi³⁺/Biochar modified electrode has a sensitivity of 36.66 ± 0.27 (n=3) with a relative standard deviation of 0.74% and Bi₅O₇NO₃ 15% Wt Bi³⁺/Biochar modified electrode has a sensitivity of 39.5 ± 1.0 with R.S.D of 2.61% which is higher among Biochar modified electrodes and double the value of bare electrode's sensitivity.

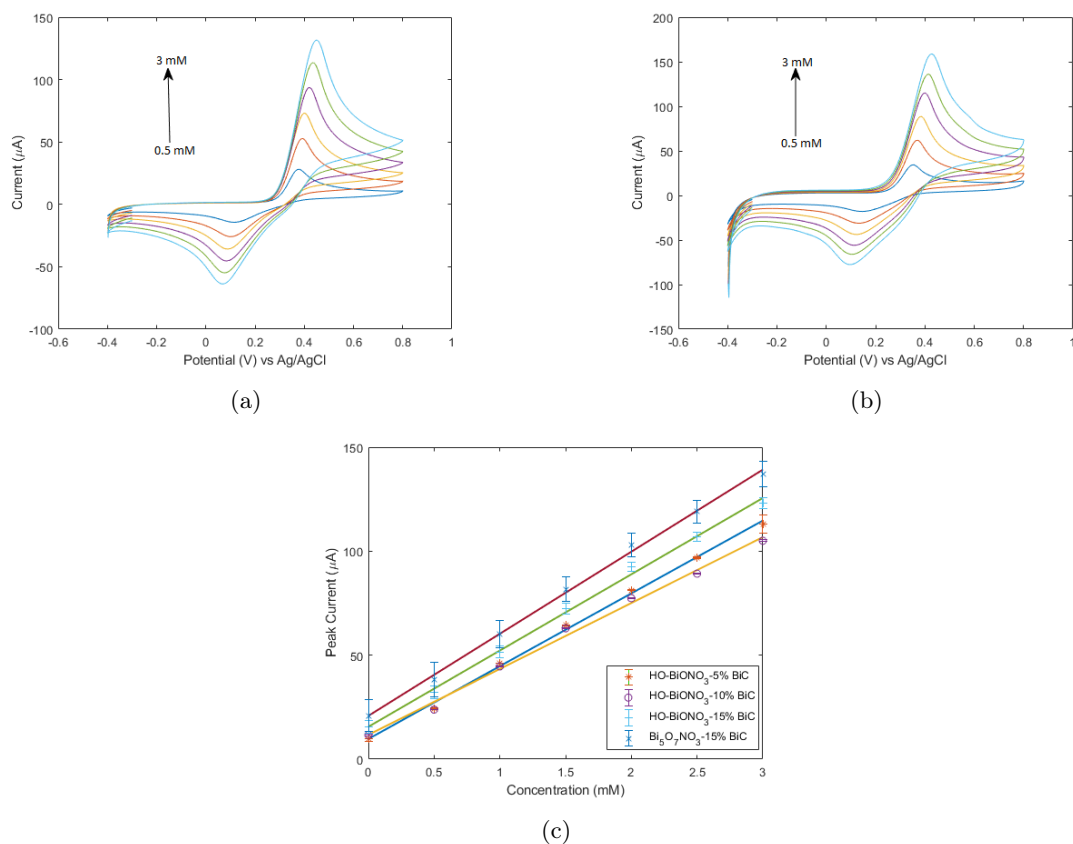


Figure 3.17: Cyclic voltammograms of 0.5mM to 3mM ($n=3$) paracetamol in 0.1M PBS pH 7 at a scan rate of 100 mV/s with (a) HO-BiONO₃ 5% Wt Bi³⁺/Biochar, (b) Bi₅O₇NO₃ 15% Wt Bi³⁺/Biochar modified electrodes, and (c) Calibration curves for Bi³⁺/Biochar modified SPEs.

Material	I_p (μA)	R^2 ($n=3$)
HO-BiONO ₃ 5% Wt Bi ³⁺ /Biochar	$34.99[C]+9.71$	0.998
HO-BiONO ₃ 10% Wt Bi ³⁺ /Biochar	$31.69[C]+11.69$	0.994
HO-BiONO ₃ 15% Wt Bi ³⁺ /Biochar	$36.66[C]+15.56$	0.998
Bi ₅ O ₇ NO ₃ 15% Wt Bi ³⁺ /Biochar	$39.46[C]+20.82$	0.998

Table 3.16: Linear regression equations of oxidation peak current with concentration for some Bi³⁺/Biochar modified electrodes.

Material	Sensitivity ($\mu A/mM$)	R.S.D($n=3$)
HO-BiONO ₃ 5% Wt Bi ³⁺ /Biochar	35.0 ± 1.2	3.57%
HO-BiONO ₃ 10% Wt Bi ³⁺ /Biochar	31.69 ± 0.16	0.50%
HO-BiONO ₃ 15% Wt Bi ³⁺ /Biochar	36.66 ± 0.27	0.74%
Bi ₅ O ₇ NO ₃ 15% Wt Bi ³⁺ /Biochar	39.5 ± 1.0	2.61%

Table 3.17: Sensitivities of some Bi³⁺/Biochar modified electrodes.

Since, it was observed with one electrode an increment in oxidation currents out of curiosity other electrodes also tested. With time all other electrodes also have different results with higher oxidation currents compared to initial measurements as we observe in figure 3.18. Different electrodes

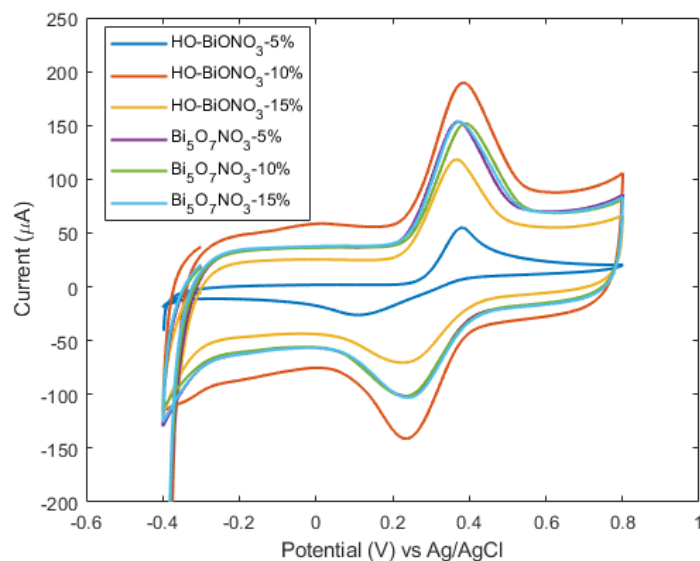


Figure 3.18: Cyclic voltammograms of 1 mM paracetamol in 0.1M PBS pH 7 at a scan rate of 100 mV/s after measurements with Bi^{3+} /Biochar modified electrodes (shown in legend).

Material	Potential (mV)	Current (μA)
HO-BiONO ₃ 5% Wt Bi^{3+} /Biochar	381.32	47.49
HO-BiONO ₃ 10% Wt Bi^{3+} /Biochar	383.76	119.97
HO-BiONO ₃ 15% Wt Bi^{3+} /Biochar	364.23	81.53
$\text{Bi}_5\text{O}_7\text{NO}_3$ 5% Wt Bi^{3+} /Biochar	369.11	102.77
$\text{Bi}_5\text{O}_7\text{NO}_3$ 10% Wt Bi^{3+} /Biochar	388.64	101.25
$\text{Bi}_5\text{O}_7\text{NO}_3$ 15% Wt Bi^{3+} /Biochar	371.55	102.35

Table 3.18: Measured potentials and currents observed in after measurements.

showed different CVs compared to initial CVs reported except HO-BiONO₃ 5% Wt Bi^{3+} /Biochar modified electrode. All the potentials and peak currents after being reported in table 3.18 and these values are uncomparable with initial values. Due to these changes in CVs, it was not possible to do blank measurements to calculate the limit of detection of these electrodes.

This is a bit tricky to understand the chemistry and why they have increased oxidation currents. It could be due to the change on the surface of the working electrode as we notice figure 3.5d and it is also completely different from other surfaces of the working electrodes we have seen. This change might have happened on the surface of other working electrodes also hence they have behaved differently. This instability can be due to the contamination of the surface or changes in temperature since all the measurements have been performed under atmospheric conditions and all the electrodes were stored in ambient air conditions after each use.

Chapter 4

Conclusions

Successful synthesis of 12 different Bismuth based composites has been done for this thesis work such as HO-BiONO₃ with and without surfactants like polyethelyne glycol (PEG) and polyvinyl butyral (PVB), Bi₅O₇NO₃, and Bi³⁺ coated BioChar (black carbon which was already produced by pyrolysis at 1000⁰C). Scanning electron microscopic experiments showed that some materials have rod shaped structure with uniform distribution and some others in spherical structure by the formation of aggregates.

The development of new electrochemical sensors has been done by modifying working electrodes surfaces of commercially available screen-printed carbon electrodes under ambient atmospheric conditions using homogeneous suspensions of different synthesized materials. SEM images of the surfaces of working electrodes have shown that the particles were broken into smaller sizes with rectangular and cubic shapes. These sensors were tested by cyclic voltammetric experiments to determine 1mM paracetamol in 0.1M PBS at psychological pH of 7 at a scan rate of 100 mV/s. All newly developed sensors were performing better than the unmodified screen-printed electrode in terms of overpotential and redox peak currents. Then cyclic voltammetry was performed by varying the scan rate and found that the electrochemical system was a freely diffusing quasi-reversible system. Redox peak currents were varying linearly with the square root of the scan rate and redox peak positions are shifting with scan rate. Peak to peak separation ΔE_p was calculated by taking the difference between anodic and cathodic peak positions, and half potential $E_{1/2}$ was calculated by taking the average between anodic and cathodic peak positions at a scan rate of 100 mV/s. Redox peak positions and ΔE_p were varying linearly with the natural logarithm of scan rate. Electron transfer coefficient α , electron transfer number (n), and kinetic rate constant (k) at a scan rate of 100 mV/s were calculated with the help of the Laviron model. The electron transfer number (n) was found matching with the number of electrons participating in the redox mechanism of paracetamol which was verified by comparing with the literature. The diffusion coefficient (D) of paracetamol at a scan rate of 100 mV/s was also calculated by taking the electroactive area equal to the geometrical area of the working electrode with the help of Randles-Sevcik equation. Among 12 newly developed sensors, the PEG-coated HO-BiONO₃ sensor was found with the higher oxidation peak current, low oxidation peak potential at a scan rate of 100 mV/s. It also has shown a high kinetic rate constant (k) of 58.2 ms⁻¹ meaning that it was involved in the faster reaction and has a high chance of reversible reaction due to it's less ΔE_p of 224.6 mV. And the sensors with less ΔE_p have a high rate constant and involves in faster reactions and with high ΔE_p have low rate constant and slow reactions. Hence, the rate constant is inversely proportional to the peak to peak separation of ΔE_p in the Laviron model. ΔE_p was increasing as the concentration of the analyte increases due to the presence of uncompensated resistance due to the high concentration of the analyte.

Cyclic voltammetry was performed by varying the concentration of paracetamol from 0.5mM to 3mM to find the sensitivity of newly developed sensors. All newly developed sensors showed a good linear relationship for the oxidation peak current with the paracetamol concentration ranging from 0.5mM to 3mM. Then by taking the oxidation peak currents with concentration calibration curves were constructed. The sensitivity of sensors was calculated from the slopes of calibration curves and the limit of detection (LOD) was calculated from the relation between LOD, sensitivity, and standard deviation of blank measurements. The best sensitivity was found for PEG-coated HO-BiONO₃ sensor which has $43.50 \pm 0.54 \mu\text{A}/\text{mM}$ with a relative standard deviation of 1.24% and has a LOD of 2.235 ± 0.028 . The best LOD was found for PEG and PVB coated HO-BiONO₃ sensor which has LOD of 1.48763 ± 0.00037 and sensitivity of 36.511 ± 0.011 with a relative standard deviation of 0.03%.

Inspired by the literature, a cleaning procedure was followed with the help of low concentrated H₂SO₄. Interestingly there was an increment in oxidation peak current after cleaning in H₂SO₄ but this effect was immediate and SEM image of the surface of the working electrode has shown that the surface has a high density of particles with small sizes by forming aggregates. For Bi³⁺/BioChar modified sensors the oxidation current has been increased with time and the peak currents with initial measurements and after measurements are reported. Also, the SEM image of the surface has shown a clear change on the surface of the electrode. It has been also observed that size and morphology of the particles played a significant role on the performance of the newly developed electrochemical sensors. Further study on the interaction between Bismuth-composites and paracetamol by EDS measurements and electrochemical analysis by calculating the specific surface area of the particles has been planned for the future.

Bibliography

- [1] Jaison Jeevanandam, Ahmed Barhoum, Yen S. Chan, Alain Dufresne, and Michael K. Danquah. Review on nanoparticles and nanostructured materials: history, sources, toxicity and regulations. *Beilstein Journal of Nanotechnology*, 9:1050–1074, 2018. doi: doi:10.3762/bjnano.9.98.
- [2] Miroslav Pohanka and Petr Skládal. Electrochemical biosensors – principles and applications. *Journal of Applied Biomedicine*, 6:57–64, 2008.
- [3] A. Rasooly and K.E. Herold. *Biosensors and Biodetection, Methods and Protocols*. Rasooly, A., Herold, K.E., Eds.; Humana Press, New York, NY, USA, 2009.
- [4] S. Andreescu and O.A. Sadik. Trends and challenges in biochemical sensors for clinical and environmental monitoring. *Pure Appl. Chem*, 76:861–878, 2004. doi: <https://doi.org/10.1351/pac200476040861>.
- [5] A. Zuzuarregui, D. Souto, E. Perez-Lorenzo, S. Sanches-Gomez, G. Martinez de Tejera, K. Brandenburg, S. Arana, and M. Mujika. Novel integrated and portable endotoxin detection system based on an electrochemical biosensor. *Analyst*, 140:654–660, 2015.
- [6] Keiichiro Yamanaka, Mun’delanji C. Vestergaard, and Eiichi Tamiya. Printable Electrochemical Biosensors: A Focus on Screen-Printed Electrodes and Their Application. *Sensors*, 16(1761), 2016. doi: doi:10.3390/s16101761.
- [7] A. Washe, P. Lozano-Sanchez, and D. Bejarano-Nosas. Facile and versatile approaches to enhancing electrochemical performance of screen printed electrodes. *Electrochim. Acta*, 91:166–172, 2013.
- [8] T.N.T. Lien, Y. Takamura, E. Tamiya, and M.C. Vestergaard. Modified screen printed electrode for development of a highly sensitive label-free impedimetric immunosensor to detect amyloid beta peptides. *Anal. Chim. Acta*, 892:69–76, 2015.
- [9] R. Khan, W. Gorski, and C.D. Garcia. Nanomolar Detection of Glutamate at a Biosensor Based on Screen-Printed Electrodes Modified with Carbon Nanotubes. *Electroanalysis*, 10:2357–2363, 2011.
- [10] B. Prieto-Simon, J. Macanas, M. Munoz, and E. Fabregas. Evaluation of different mediator-modified screen-printed electrodes used in a flow system as amperometric sensors for NADH. *Talanta*, 71:2102–2107, 2007.
- [11] Carrara Sandro. *Bio/CMOS Interfaces and Co-Design*. Springer, New York, NY, USA, 2013.
- [12] Noemie Elgrishi, Kelley J. Rountree, Brian D. McCrathy, Eric S. Rountree, Thomas T. Eisenhart, and Jillian L. Dempsey. A Practical beginner’s guide to Cyclic Voltammetry. *J. Chem. Educ*, 95:197–206, 2018.

- [13] Allen J. Bard and Larry R. Faulkner. *ELECTROCHEMICAL METHODS Fundamentals and Applications*. John Wiley & Sons, Inc, New York, NY, USA, 2001.
- [14] J. A. V. Butler. *Trans. Faraday Soc*, 19:729–734, 1924.
- [15] E. Laviron. General expression of the linear potential sweep voltammogram in the case of diffusionless electrochemical systems. *J. Electroanal. Chem.*, 101:19–28, 1979.
- [16] Michael J. Honeychurch. Effect of the interfacial potential distribution on the measurement of the rate constant for electron transfer between electrodes and redox adsorbates. *Langmuir*, 14:6291–6296, 1998.
- [17] R.M.D. Carvalho, R.S. Freire, S. Rath, and L.T. Kubota. *J. Pharm. Biomed. Anal.*, 34(871), 2004.
- [18] Wang S, Xie F, and Hu R. *Sens Actuators B*, 123:495–500, 2007.
- [19] Xinhuang Kang, Jun Wang, Hong Wu, Jun Liu, Ilhan A. Aksay, and Yuehe Lin. A graphene-based electrochemical sensor for sensitive detection of paracetamol. *Talanta*, 81:754 – 759, 2010.
- [20] M. Li and L.H. Jing. *Electrochim. Acta*, 52(3250), 2007.
- [21] Filik H and Tavman A (2007). *J Anal Chem*, 62:530–535, 2007.
- [22] Trojanowicz M. *Flow injection analysis: instrumentation and applications*. World Scientific, Singapore, 2000.
- [23] Burgot G, Auffret F, and Burgot JL. *Anal Chim Acta*, 343:125–141, 1997.
- [24] Satinsky D, Neto I, Solich P, Sklenarova H, Conceicao M, and Montenegro BSM. *J Sep Sci*, 27:529–536, 2004.
- [25] D. Easwaramoorthy, Y.C. Yu, and H.J. Huang. *Anal. Chim. Acta*, 95(439):129–141, 2001.
- [26] Yang B, Mo J, Yang X, and Wang L. *J Instrum Anal*, 19:13–15, 2000.
- [27] Hilton MJ and Thomas KV. *J Chromatogr A*, 1015:129–141, 2003.
- [28] Zarei AR, Afkhami A, and Sarlak N. *J AOAC Int*, 88(439):1695–1701, 2005.
- [29] Xiaodong ShangGuan, Hongfang Zhang, and Jianbin Zheng. Electrochemical behavior and differential pulse voltammetric determination of paracetamol at a carbon ionic liquid electrode. *Anal Bioanal Chem*, 391:1049–1055, 2008.
- [30] Mohammed Zidan, Tan Wee Tee, Abdul Halim Abdullah, Zulkarnain Zainal, and Goh Joo Kheng. Electrochemical oxidation of paracetamol mediated by nanoparticles bismuth oxide modified glassy carbon electrode. *Int. J. Electrochem. Sci*, 6:279 – 288, 2011.
- [31] Ilona Sadok, Katarzyna Tyszczyk-Rotko, and Agnieszka Nosal-Wiercinska. Bismuth particles nafion covered boron-doped diamond electrode for simultaneous and individual voltammetric assays of paracetamol and caffeine. *Sensors and Actuators B*, 235:263–272, 2016.
- [32] Pablo Fanjul-Boladoa, Pedro Josee Lamas-Ardisanab, David Hernandez-Santosa, and Agustin Costa-Garcia. Electrochemical study and flow injection analysis of paracetamol in pharmaceutical formulations based on screen-printed electrodes and carbon nanotubes. *Analytica Chimica Acta*, 638:133–138, 2009.

- [33] Zhiyin Xiao, Chaoting Xu, Xiaohong Jiang, Wenlong Zhang, Yuxuan Peng, Rujia Zou, Xiaojuan Huang, Qian Liu, Zongyi Qin, and Junqing Hu. Hydrophilic bismuth sulfur nanoflower superstructures with an improved photothermal efficiency for ablation of cancer cells. *Nano Research*, 9(7):1934–1947, 2016.
- [34] Yong Wang, Yongyou Wu, Yujing Liu, Jia Shen, Ling Lv, Liubing Li, Liecheng Yang, Jianfeng Zeng, Yangyun Wang, Leshuai W. Zhang, Zhen Li, Mingyuan Gao, and Zhifang Chai. Bsa-mediated synthesis of bismuth sulfide nanotheranostic agents for tumor multimodal imaging and thermoradiotherapy. *Adv. Funct. Mater.*, 26:5335 – 5344, 2016.
- [35] Zhenglin Li, Jing Liu, Ying Hu, Zhuo Li, Xuelei Fan, Ye Sun, Flemming Besenbacher, Chunying Chen, and Miao Yu. Biocompatible pegylated bismuth nanocrystals: “all-in-one” theranostic agent with triple-modal imaging and efficient in vivo photothermal ablation of tumors. *Biomaterials*, 141:284 – 295, 2017.
- [36] Juan Li, Fei Jiang, Bo Yang, Xiao-Rong Song, Yan Liu, Huang-Hao Yang, Dai-Rong Cao, Wen-Rong Shi, and Guo-Nan Chen. Topological insulator bismuth selenide as a theranostic platform for simultaneous cancer imaging and therapy. *SCIENTIFIC REPORTS*, 3(1998):1 – 7, 2013. doi: DOI:10.1038/srep01998.
- [37] Hao Huang, Lizhen He, Wenhua Zhou, Guangbo Qu, Jiahong Wang, Na Yang, Jie Gao, Tianfeng Chen, Paul K. Chu, and Xue-Feng Yu. Stable black phosphorus/Bi₂O₃ heterostructures for synergistic cancer radiotherapy. *Biomaterials*, 171:12 – 22, 2018.
- [38] H. Z. Sun. *Biological Chemistry of Arsenic, Antimony and Bismuth*. Wiley, Chichester, West Sussex, UK, 2011.
- [39] K. D. Mjos and C. Orvig. Metallo drugs in medicinal inorganic chemistry. *Chem. Rev.*, 114: 4540 – 4563, 2016.
- [40] Gen-qing Liu, Hui Zhonga, Xiao-rong Lia, Kai Yanga, Fei-fei Jiaa, Zhi-peng Chenga, Lili Zhanga, Jing-zhou Yina, Li-ping Guoc, and Hai yan Qian. Research on nonenzymatic electrochemical sensor using HO-BiONO₃ nanocomposites for glucose detection. *Sensors and Actuators B*, 242:484 – 491, 2017.
- [41] Shujie Yu, Gaoke Zhang, Yuanyuan Gao, and Baibiao Huang. Single-crystalline bi₅o₇no₃ nanofibers: Hydrothermal synthesis, characterization, growth mechanism, and photocatalytic properties. *Journal of Colloid and Interface Science*, 354:322–330, 2011.
- [42] S. K. K. Jatkar D. N. Mehta. *J. Indian Inst. Sci*, 18A:85, 1935.
- [43] K. Schwabe. *Z. Elektrochem*, 53:125, 1949.
- [44] K. Schwabe. *Z. Elektrochem*, 55:411, 1951.
- [45] Ivan Svancara, Chad Prior, Samo B. Hocevar, and Joseph Wang. A decade with bismuth-based electrodes in electroanalysis. *Electroanalysis*, 22(13):1405–1420, 2010.
- [46] Joseph Wang, Jianmin Lu, Samo B. Hocevar, and Percio A. M. Farias. Bismuth-coated carbon electrodes for anodic stripping voltammetry. *Anal. Chem.*, 72(14):3218–3222, 2000.
- [47] E. A. Hutton, B. Ogorevc, S. B. Hocevar, F. Weldon, M. R. Smyth, and J. Wang. An introduction to bismuth film electrode for use in cathodic electrochemical detection. *Anal. Chem.*, 3(12):707–711, 2001. doi: [https://doi.org/10.1016/S1388-2481\(01\)00240-5](https://doi.org/10.1016/S1388-2481(01)00240-5).
- [48] Joseph Wang, Jianmin Lu, Samo B. Hocevar, and Bozidar Ogorevc. Bismuth-coated screen-printed electrodes for stripping voltammetric measurements of trace lead. *Electroanalysis*, 13(1):13–16, 2001.

- [49] Karel Vytras, Ivan Svancara, and Radovan Metelka. A novelty in potentiometric stripping analysis: Total replacement of mercury by bismuth. *Electroanalysis*, 14(19-20):1359–1364, 2002.
- [50] Agnieszka Krolicka, Andrzej Bobrowski, Kurt Kalcher, Jan Mocak, Ivan Svancara, and Karel Vytras. Study on catalytic adsorptive stripping voltammetry of trace cobalt at bismuth film electrodes. *Electroanalysis*, 15(23-24):1859–1863, 2003.
- [51] A. T. Maghasi, H. B. Halsall, W. R. Heineman, and H. L. R. Rilo. Detection of secretion from pancreatic islets using chemically modified electrodes. *Anal. Biochem*, 326(2):183–189, 2004.
- [52] N. A. Malakhova, N. Yu. Stojko, and Kh. Z. Brainina. Novel approach to bismuth modifying procedure for voltammetric thick film carbon containing electrodes. *Electrochem. Commun*, 9(2):221–227, 2007.
- [53] O. El Tall, D. Beh, N. Jaffrezic-Renault, and O. Vittori. Electroanalysis of some nitro-compounds using bulk bismuth electrode. *Intern. J. Environ. Anal. Chem*, 90(1):40–48, 2010.
- [54] D. Ma, Y. Zhao, J.Z. Zhao, Y.W. Li, Y. Lu, and D.J. Zhao. Aqueous synthesis of hierarchical bismuth nanobundles with high catalytic activity to organic dyes. *Superlattices Microstruct*, 83:411 – 421, 2015.
- [55] M.A. Chamjangali, H. Kouhestani, F. Masdarolomoor, and H. Daneshinejad. A voltammetric sensor based on the glassy carbon electrode modified with multi-walled carbon nanotube/poly(pyrocatechol violet)/bismuth film for determination of cadmium and lead as environmental pollutants. *Sens. Actuators B*, 216:384 – 393, 2015.
- [56] D. Agustini, A.S. Mangrich, M.F. Bergamini, and L.H. Marcolino-Junior. Sensitive voltammetric determination of lead released from ceramic dishes by using bismuth nanostructures anchored on biochar. *Talanta*, 142:221 – 227, 2015.
- [57] C.V. Horst, B. Silwana, E. Iwuoha, and V. Somerset. Bismuth-silver bimetallic nanosensor application for the voltammetric analysis of dust and soil samples. *J. Electroanal. Chem*, 752: 1 – 11, 2015.
- [58] Nima Aliakbarinodehi, Irene Taurino, Jagdale Pravin, Alberto Tagliaferro, Gianluca Piccinini, Giovanni De Micheli, and Sandro Carrara. Electrochemical nanostructured biosensors: carbon nanotubes versus conductive and semi-conductive nanoparticles. *Chemical Papers*, 69(1): 134–142, 2015. doi: DOI:10.1515/chempap-2015-0004.
- [59] M. Karbalaeei, M. Seifi, and H. Sheibani. Regioselective ring opening of 2,2-dicyano oxiranes by 1,3-dinucleophiles in the presence of lewis acids such as bismuth(iii) nitrate pentahydrate $[\text{bi}(\text{no}_3)_3 \cdot 5\text{h}_2\text{o}]$ and zirconium(iv)chloride (zrcl_4). *Res. Chem. Intermed*, 41:4679–4686, 2015.
- [60] Hiroshi Kodama. Synthesis of new compound $\text{Bi}_5\text{O}_7\text{NO}_3$, by thermal decomposition. *Journal of Solid State Chemistry*, 112:27–30, 1994.
- [61] Surinder K. Mehtaa, Khushboo, and Ahmad Umarb. Highly sensitive hydrazine chemical sensor based on mono-dispersed rapidly synthesized PEG-coated ZnS nanoparticles. *Talanta*, 85:2411– 2416, 2011.
- [62] Aoife Morrin, Anthony J. Killard, and Malcolm R. Smyth. Electrochemical characterization of commercial and home-made screen-printed carbon electrodes. *Analytical Letters*, 36(9): 2021–2039, 2003. doi: DOI:10.1081/AL-120023627.